NASA CR-165,461

CML 82-4 NASA CR165461

DYNAMIC RESPONSES OF A GRAPHITE/EPOXY LAMINATED BEAM TO IMPACT OF ELASTIC SPHERES

by

C.T. Sun and T. Wang

September 1982

COMPOSITE MATERIALS LABORATORY

PURDUE UNIVERSITY
School of Aeronautics and Astronautics
West Lafayette, Indiana 47907

CML 82-4 NASA CR165461

DYNAMIC RESPONSES OF A GRAPHITE/EPOXY LAMINATED BEAM TO IMPACT OF ELASTIC SPHERES

by

C.T. Sun and T. Wang

September 1982

1. Report No.	2. Government Accession No.	3. Recipient's Catalog No.
NASA CR 165461		

4. Title and Subtitle	5. Report Date
Dynamic Responses of a Graphite/Epoxy Laminated Beam to Impact of Elastic Spheres	August 1981
	6. Performing Organization Code

7. Author(s)	8. Performing Organization Report No.
C. T. Sun and T. Wang	
	10. Work Unit No.

9. Performing Organization Name and Address	11. Contract or Grant No.
Purdue University School of Aeronautics and Astronautics West Lafayette, IN 47907	NSG 3185
	13. Type of Report and Period Covered

12. Sponsoring Agency Name and Address	13. Type of Report and Period Covered
National Aeronautics and Space Administration Washington DC 20546	Topical Report
	14. Sponsoring Agency Code

15. Supplementary Notes C. C. Chamis, Structures & Mechanical Technologies Division
NASA Lewis Research Center
21000 Brookpark Road
Mail Stop 49-6
Cleveland, OH 44135

16. Abstract

Wave propagation in $[90/45/90/-45/90]_{2s}$ and $[0/45/0/-45/0]_{2s}$ laminates of a graphite/epoxy composite due to impact of a steel ball was investigated experimentally and also by using a high order beam finite element. Dynamic strain responses at several locations were obtained using strain gages. The finite element program which incorporated statically determined contact laws was employed to calculate the contact force history as well as the target beam dynamic deformation. The comparison of the finite element solutions with the experimental data indicated that the static contact laws for loading and unloading (developed under this grant) are adequate for the dynamic impact analysis. It was found that for the $[0/45/0/-45/0]_{2s}$ laminate which has a much larger longitudinal bending rigidity, the use of beam finite elements is not suitable and plate finite element should be used instead.

17. Key Words (Suggested by Author(s))	18. Distribution Statement
composite laminate, graphite/epoxy, contact law, impact, wave propagation, finite element, beams, structural dynamics.	Unclassified, Unlimited

19. Security Classif. (of this report)	20. Security Classif. (of this page)	21. No. of Pages	22. Price*
Unclassified	Unclassified		

* For sale by the National Technical Information Service, Springfield, Virginia 22161

TABLE OF CONTENTS

LIST OF FIGURES

NOMENCLATURE

A_{ij} = Laminate stiffness matrix

E_1 = Young's modulus in 1 - (fiber) direction

E_2 = Young's modulus in 2 - (transverse) direction

F = Contact force

G_{12} = In-plane shear modulus

k = Contact coefficient

k_1 = Reloading rigidity

α = Indentation

α_o = Permanent indentation

α_m = Maximum indentation before unloading

α_{cr} = Critical identation

μ_{12} = Poisson's ratio for strain in the 2-direction when stressed in the 1-direction

1. INTRODUCTION

Due to their lack of through-the-thickness reinforcement, laminated fiber composites are susceptible to impact damage. The past effort in the study of FOD (foreign object damage) of composites can be categorized into three aspects, namely, examination of impact damage by testing, wave propagation study, and the search for new impact resistant hybrid composites. Ballistic impact tests on various composites have been conducted by many people [1-4]. Under the sponsorship of NASA Lewis Research Center, a number of aircraft engine companies have carried out full scale testings on impact of composite fan blades [5-7]. Observations made from these tests have led to some understanding of the failure modes and the impact effect on the reduction in the strength of composites.

Some authors have approached the FOD problem by studying stress wave propagation in laminated composites [8-16]. Since the impact resistant properties of composites are not pure material properties but are greatly dependent on the dynamic structural behavior, the understanding of wave propagation in composites due to impact loads is of great importance to the FOD problem.

Recently, attention has been called to the use of super-hybrid composites as a possible solution to the FOD problems [17]. As the search for highly impact-resistant composites continues, the need for better testing procedures and accurate analytical models remains.

Since the impact phenomenon involves both material response at the contact zone and the structural response in the form of stress waves, it is desirable to separate these two. In the past, the classical Hertzian contact law was used to calculate the contact force which was then used as the forcing function in the analysis of the subsequent

dynamic response of the structure after an impact [12, 13, 15]. Recently, Yang and Sun [18] have conducted indentation tests on a graphite/epoxy laminate using spherical indenters and concluded that the classical Hertzian law is not valid. In particular, they found that the permanent deformation at the contact zone is very large and that the unloading path substantially deviates from the loading path. Based upon experimental data, the loading and unloading contact behaviors were modeled in terms of power laws. Since these contact laws were established based on static indentation tests, the validity of these laws in the dynamic impact analysis remains to be verified.

The purpose of this study was to conduct dynamic impact experiments to provide a basis for comparison with the analytical solution using these static contact laws.

2. Material Properties and Contact Laws

The graphite/epoxy laminates were provided by NASA Lewis Research Center. Specimens were cut from $[0/45/0/-45/0]_{2s}$ panels of 28 cm x 23 cm x 0.254 cm. When cut in the transverse direction, $[90/45/90/-45/90]_{2s}$ laminate specimens were obtained.

The ply elastic constants E_1, E_2, G_{12}, and ν_{12} were determined experimentally by an indirect procedure. According to the classical lamination theory, for a symmetric and balanced laminate, we have

$$N_x = A_{11}\,\varepsilon_{xx} + A_{12}\,\varepsilon_{yy} \tag{1}$$

$$N_y = A_{12}\,\varepsilon_{xx} + A_{22}\,\varepsilon_{yy} \tag{2}$$

where N_x and N_y are the in-plane forces in the x- and y- direction, respectively. ε_{xx} and ε_{yy} are the normal strains, and A_{ij} are elements of the plate in-plane stiffness matrix [19]. The quantities A_{ij} are functions of the ply elastic constants as well as the fiber orientation.

Simple tension specimens of 2.54 cm width were cut from the large panels into $[0/45/0/-45/0]_{2s}$ and $[90/45/90/-45/90]_{2s}$ laminates. Uniaxial tension tests ($N_x \neq 0$, $N_y = 0$) were then performed and the longitudinal and transverse strains were measured. With the two types of specimens, four equations in the form of Eqs. (1) and (2) were obtained from the experimental data. Since these equations are highly nonlinear in the elastic constants, a numerical iterative procedure was used to find the solution. The results are

$$E_1 = 120 \text{ GPa } (17.5 \times 10^6 \text{ psi})$$
$$E_2 = 7.9 \text{ GPa } (1.15 \times 10^6 \text{ psi})$$
$$G_{12} = 5.5 \text{ GPa } (0.8 \times 10^6 \text{ psi}) \qquad (3)$$
$$\nu_{12} = 0.30$$

The contact laws used in this study were obtained by Yang and Sun [18]. For the loading process, the contact force F and the indentation α have the relation

$$F = k\,\alpha^{3/2} \qquad (4)$$

where k is a contact coefficient whose value depends on the target material properties and the identer size. For the graphite/epoxy laminate under consideration we have

$$k = 3.36 \times 10^4 \text{ N/mm}^{1.5} \quad (9.7 \times 10^5 \text{ lb/in.}^{1.5}) \qquad (5)$$

for the 12.7 mm (0.5) in.) diameter steel identer, and

$$k = 0.94 \times 10^4 \text{ N/mm}^{1.5} \; (5.6 \times 10^5 \text{ lb/in.}^{1.5}) \qquad (6)$$

for the 6.35 mm (0.25 in.) diameter indenter.

The unloading process is modeled by the following equation

$$F = F_m \left[\frac{\alpha - \alpha_o}{\alpha_m - \alpha_o}\right]^{2.5} \qquad (7)$$

where F_m is the contact force corresponding to the indentation α_m where unloading starts, and α_o is the corresponding depth of the permanent crater. The following formula was suggested by Yang and Sun [18] for computing α_o:

$$\alpha_o/\alpha_m = 1 - (\alpha_{cr}/\alpha_m)^{2/5} \tag{8}$$

with

$$\alpha_o = 0 \text{ if } \alpha_m \leq \alpha_{cr} \tag{9}$$

In Eq. (8), the parameter α_{cr} is constant for both sizes of indenter. For this graphite/epoxy,

$$\alpha_{cr} = 8.0 \times 10^{-2} \text{ mm} \tag{10}$$

The reloading behavior is modeled by

$$F = k_1(\alpha - \alpha_o)^{3/2} \tag{11}$$

in which

$$k_1 = F_m/(\alpha_m - \alpha_o)^{3/2} \tag{12}$$

is the reloading rigidity. This formula has been experimentally verified by Yang and Sun [18].

A higher order beam finite element with six degrees of freedom was used in conjunction with the contact laws for the dynamic impact analysis. A complete listing of this program can be found in [20]. This program is able to calculate the transient contact force, the dynamic deformation, and stresses in the beam under any impact condition. For all the numerical solutions, the beam was modeled with finite elements of size 6.25 mm and a 0.2×10^{-6} sec. time increment was chosen for the time integration. This finite element size and time increment have been tested and found to yield convergent solutions.

3. Experimental Procedures

The schematic diagram for the experimental set-up is shown in Fig. 1. A pendulum with a steel ball of 12.7 mm diameter was used as the impactor for low velocity impact (below 5 m/sec), and an air gun was used to shoot a 6.35 mm diameter steel ball for high velocity impacts. By adjusting the pressure of the compressed air in the chamber of the air gun the velocity of the projectile ranges from 20 m/sec to 100 m/sec.

Two light emitting diodes (LED) and two photo detectors were used to find the velocity of the projectile. When the projectile interrupts the first light beam, a pulse is generated to start the time counter. Once the projectile cuts the second light beam, another pulse is generated to stop the counter. The velocity of the projectile is obtained by dividing the distance between the two LED's by the time registered on the counter.

Two boundary conditions were realized in the impact experiments, namely, clamped-clamped and free-free conditions. For the clamped-clamped condition, the specimen was tightly gripped to a massive stand while in the case of free-free end condition, the specimen was hung on two thin strings. Strain gages were mounted on the specimen at various locations. One gage was placed exactly on the back side of the impact point for triggering the oscilloscope which recorded the strain signals from other gages. The strain gages (EA-13-062 AQ 350) were marketed by Micro Measurement Co. and Eastman 910 was used as the bonding glue. Signals from the gages were amplified by a 3A9 Textronix amplifier and displayed on the screen of the oscilloscope.

All test specimens were approximately 25.4 mm (1 in.) wide. The length of the beam specimens ranged from 177.8 mm to 381 mm.

4. Results and Discussions

Daniel et al [14] have concluded from their transverse impact experiments that the in-plane membrane deformation is negligible. To verify this in our case, a series of tests were conducted with two strain gages mounted on the opposite faces of the laminated beam to record the longitudinal normal strain histories at a certain location. From the results presented in Figs. 2 and 3, it can be seen that the strains on the opposite sides of the beam have the same magnitudes but opposite signs. This indicates that the deformation is dominated by bending, i.e., the impact-induced motion is predominantly a flexural wave.

4.1 $[90/45/90/-45/90]_{2s}$

Figure 4 shows the typical dynamic contact force, the displacement of the impacting ball and the displacement of the beam at the impact point predicted by the finite element program along with the contact laws. The difference between the ball and beam displacements is the indentation. The multiple impacts are the results of waves reflected from the clamped ends.

In Figs. 5-7, the longitudinal surface strains at different locations on a clamped-clamped $[90/45/90/-45/90]_{2s}$ laminate subjected to impact of a 12.7 mm diameter steel ball are presented. The impact velocity was 3.16 m/sec. The finite element solutions seem to agree very well with the experimental data at the initial period after the wave arrives. The agreement is especially good at points closer to the impact point. After the initial wave train passes the gage

location, discrepancies between the finite element solutions and experimental results are noted.

Initially, such discrepancies were thought to be originated from the numerical instability in the finite element program. However, a study on the numerical stability indicated that the finite elements had already converged. This led to the re-examination of the boundary conditions. It was suggested that the clamped end condition as modeled by the finite elements was not actually realized in the experiment and part of the wave might have penetrated into the grips and was reflected totally as predicted by the finite element solution which exhibits a strong oscillatory behavior due to wave reflections. To verify this point, a free-free laminated beam (2.82 mm x 27.9 mm x 177.8 mm) was used. The dynamic strain history at 38.1 mm from the impact point is shown in Fig. 8. Excellent agreement between the finite element solution and the experimental data up to 400 μ sec. is noted.

More experiments with a free-free beam were then conducted. This beam was substantially longer (381 mm) than the previous one (177.8 mm). The experimentally obtained strain histories at three different locations are shown in Figs. 9-11. It is evident that the experimental results also show a pronounced oscillatory behavior as predicted by the finite element solutions, although of a lesser magnitude. This smaller strain magnitude at the later time could be due to material damping which has not been taken into account in the finite element solution. It is also noted that the wave predicted by the finite element solution travels at a slightly lower velocity than the measured value. This could be due to the fact that the displacement-formulated finite element tends to be stiffer than the actual structure.

The results for higher impact velocities (in the range of 30 m/sec) are shown in Figs. 12-15. From Fig. 12, it is noted that at higher impact velocities, multiple impacts exist no more. The basic characteristics are similar to those at lower impact velocities.

4.2 $[0/45/0/-45/0]_{2s}$ Graphite/Epoxy Beam

Unlike the $[90/45/90/-45/90]_{2s}$ laminated beam, the $[0/45/0/-45/0]_{2s}$ laminated beam has much greater bending rigidity in the longitudinal direction. It would take longer time for waves to travel across the width of the specimen. As a result, the use of beam finite element to model the specimen (25.4 mm wide) may not be adequate.

For this type of laminate, the specimen was clamped at both ends during the impact test. The impact force was calculated by using the finite element program with the result shown in Figs. 16-17 for low and high impact velocities, respectively.

Figure 18 shows the strain response at a location 38.1 mm from the impact point on a beam of dimensions 2.72 mm x 27.7 mm x 228.6 mm subjected to impact of a 12.7 mm diameter steel ball. The impact velocity is 3.16 m/sec. Figures 19-21 present the strain histories at three different locations on a beam of similar dimensions under the same impact condition. From these results, it is clear that, although the finite element solutions yield the same trend, they predict higher peak strain magnitudes than the experimental data.

The results for higher impact velocities are shown in Figs. 22-25. Two phenomena are readily observed. First, the wave is reflected and returns much faster due to the higher bending rigidity of the beam.

Second, there seems to be a wave of significant magnitude traveling in the width-direction that is reflected by the free edges and returns to interact with the main flexural wave in the longitudinal direction. The hump in the strain curve for the point located at 38.1 mm from the impact point (at 50 μ sec after impact) could be attributed to the arrival of the transverse flexural wave. Indeed, if plate finite elements are used, the analytical solution also exhibits such behavior. The plate finite element solution will be discussed in a forthcoming report.

4.3 Span Effect

To further study the phenomenon of the longitudinal reflected waves, several experiments with specimens of different lengths were conducted. Fig. 26 shows the experimental results for two $[90/45/90/-45/90]_{2s}$ laminated beams of 203.2 mm and 355.6 mm in length, respectively. These beams were clamped at both ends and were subjected to impact of a 6.35 mm steel ball at a velocity of 30 m/sec. It is evident that initially before the reflected wave arrives, the strains in these two beams are identical.

Fig. 27 shows the experimental results for two $[90/45/90/-45/90]_{2s}$ laminated beam subjected to impact at a lower velocity (3.16 m/sec). The results for the $[0/45/0/-45/0]_{2s}$ laminated beam are presented in Fig. 28. Again, the same conclusion can be drawn.

5. Conclusions

Experiments were conducted to study flexural wave propagation in a graphite/epoxy lamianted composite. Both $[90/45/90/-45/90]_{2s}$ and $[0/45/0/-45/0]_{2s}$ laminates were used in these experiments. Dynamic strain responses at various locations of a steel ball impact were measured by strain gages. The impact velocity considered ranges from 3 m/sec to about 37 m/sec. A finite element program which incorporated statically measured contact laws was employed to calculate the dynamic impact responses. The experimental results were compared with the finite element solutions.

The result of this study indicates that the statically determined contact laws are adequate for the dynamic impact analysis. The beam finite element is more suitable for modeling the $[90/45/90/-45/90]_{2s}$ laminate due to its higher transverse bending rigidity. The $[0/45/0/-45/0]_{2s}$ laminate, on the other hand, exhibits strong plate bending effects even for a large aspect ratio. For more accurate analytical results, plate finite elements should be used.

Acknowledgment

The authors wish to acknowledge the financial support by NASA Lewis Research Center under Grant No. NSG 3185. They are also grateful to Dr. C.C. Chamis for his interest in this work and many helpful discussions during the course of this research.

6. References

[1] Foreign Object Impact Damage to Composites, ASTM STP 568, American Society for Testing and Materials, 1973.

[2] Ross, C.A., and Sierakowski, R.L., "Studies on the Impact Resistance of Composite Plates," Composites, July 1973, pp. 157-161.

[3] Starnes, J.H., Rodes, M.D., and Williams, J.G., "The Effect of Impact Damage and Circular Holes on the Compressive Strength of a Graphite-Epoxy Laminate," NASA Technical Memorandom 78796, October, 1978.

[4] Rodes, M.D., Williams, J.G., and Starnes, J.H., "Low-Velocity Impact Damage in Graphite-Fiber Reinforced Epoxy Laminates," Proceedings, the 34th .nnual Conference, Reinforced Plastics/ Composites Institute, the Society of the Plastics Industry, Inc., New Orleans, Louisiana, 1979.

[5] Graff, J., Stoltze, L., and Varholak, E.M., "Impact Resistance of Spar-Shell Composite Fan Blades," NASA CR-134521, 1973.

[6] Premont, E.J., and Stubenranch, K.R., "Impact Resistance of Composite Fan Blades," NASA CR-134515, 1973.

[7] Oller, T.L., "Fiber Composite Fan Blade Impact Improvement Program," NASA CR-135078, 1976.

[8] Moon, F.C., "Wave Surface Due to Impact on Anisotropic Plates," Journal of Composite Materials, Vol. 6, 1972, pp. 62-79.

[9] Moon, F.C., "A Critical Survey of Wave Propagation and Impact in Composite Materials," NASA CR-121226, 1973.

[10] Moon, F.C., and Kim, B.S., "Impact Induced Stress Waves in an Anisotropic Plate," AIAA Journal, Vol. 17, No. 10, 1979, pp. 1126-1133.

[11] Sun, C.T., "Propagation of Shock Waves in Anisotropic Composite Plates," Journal of Composite Materials," Vol. 7, 1973, pp. 366-382.

[12] Sun, C.T. and Chattopadhyay, S., "Dynamic Response of Anisotropic Laminated Plates under Initial Stress to Impact of a Mass," Journal of Applied Mechanics, Vol. 42, 1975, pp. 693-698.

[13] Sun, C.T., "An Analytical Method for Evaluation of Impact Damage Energy of Laminated Composites," Composite Materials: Testing and Design (Fourth Conference), ASTM STP 617, American Society for Testing and Materials, 1977, pp. 427-440.

[14] Daniel, I.M., Liber, T., and LaBedg, "Wave Propagation in Transversely Impacted Composite Laminates," Experimental Mechanics, January 1979, pp. 9-16.

[15] Chou, P.C. and Morimer, R.W., "Impact Behavior of Polymeric Matrix Composite Plates," AFML TR-76-242, Air Force Materials Laboratory, December, 1976.

[16] Takeda, N., Sierakowski, R.L., and Malvern, L.E., "Wave Propagation Experiments on Ballistically Impacted Composite Laminates," Journal of Composite Materials, Vol. 15, 1981, pp. 99-194.

[17] Chamis, C.C., Lark, R.F., and Sullivan, T.L., "Super-Hybrid Composites - An Emerging Structural Material," Proceedings of the Third Conference on Fibrous Composites in Flight Vehicle Design, NASA TM X-3377, 1976.

[18] Yang, S.H., and Sun, C.T., "Indentation Law for Composite Laminates," Composite Materials: Testing and Design (Sixth Conference), 1981.

[19] Jones, R.M., Mechanics of Composite Materials, Scripta Book Company, 1975.

[20] Sun, C.T., and Yang, S.H., "Contact Law and Impact Responses of Laminated Composites," NASA CR-159884, 1980.

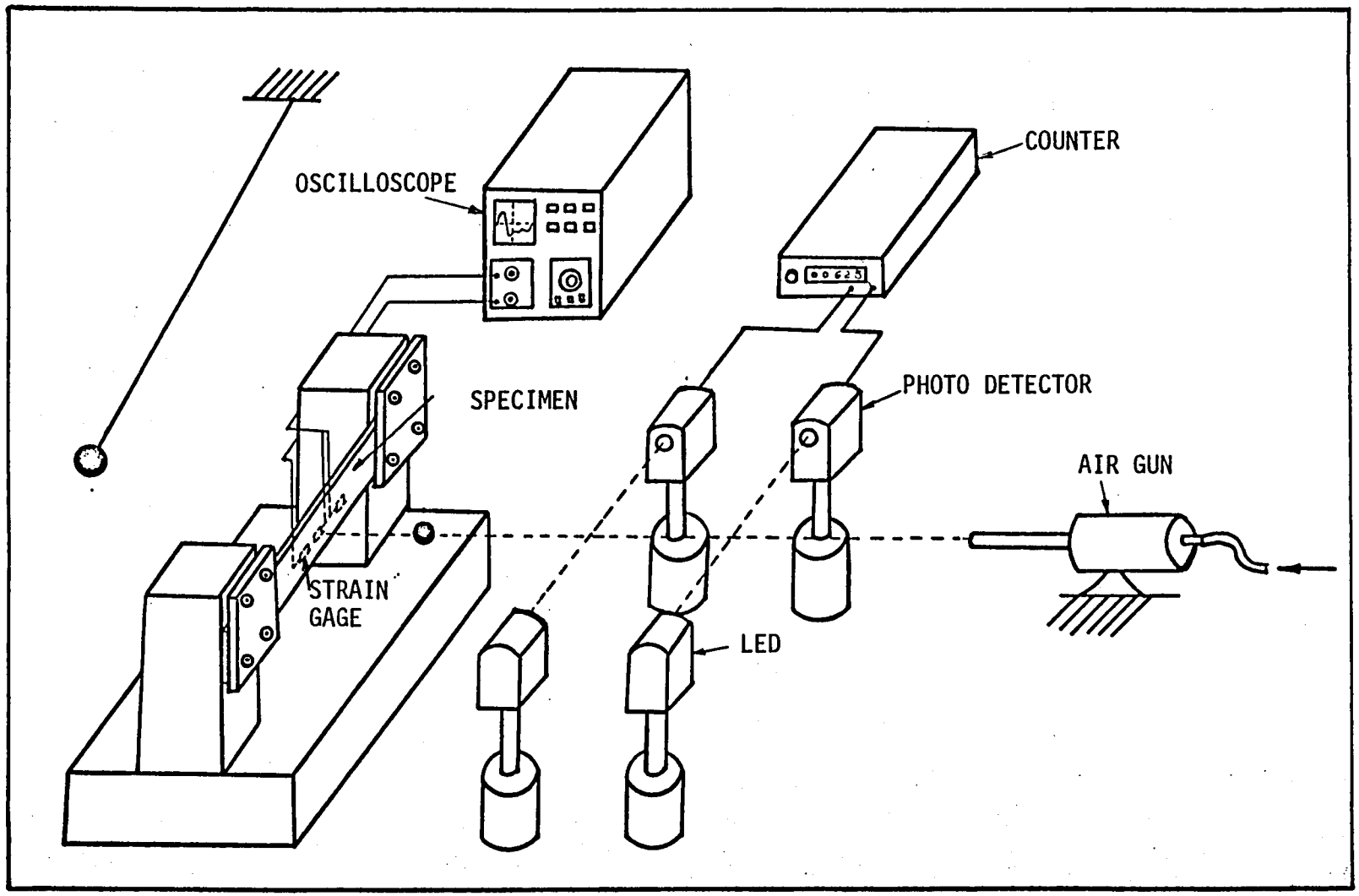

Fig. 1 Schematic Diagram of experimental apparatus.

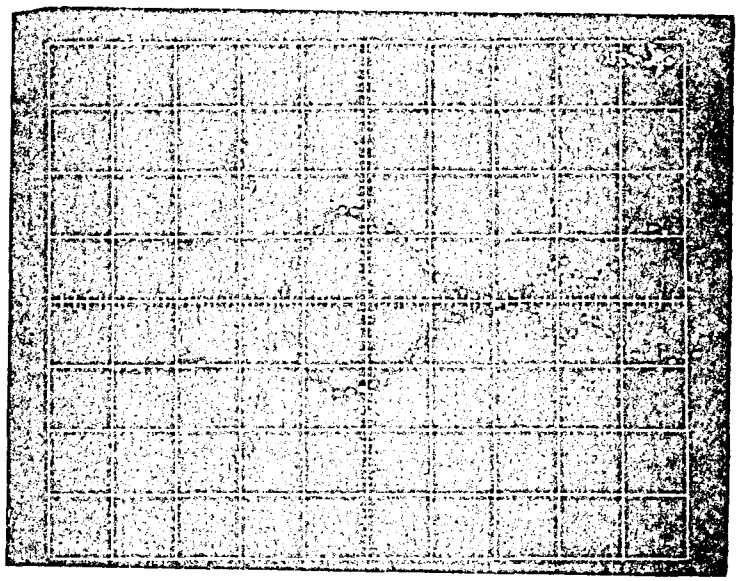

Fig. 2 Strain-gage signals on opposite faces at 38.1 mm from the impact point on the $[90/45/90/-45/90]_{2s}$ beam (2.62 mm x 27.74 mm x 228.6 mm) impacted with a 6.35 mm diameter steel ball at 31.46 m/sec.

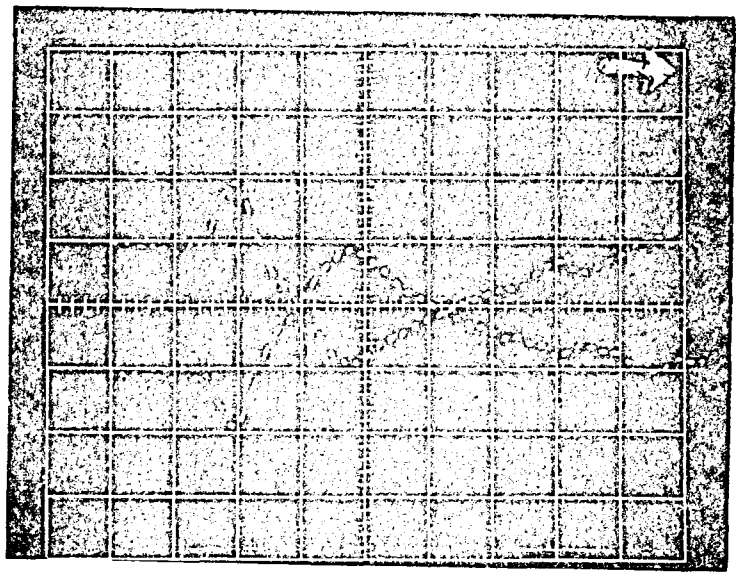

Fig. 3 Strain-gage signals on opposite faces at 38.1 mm from the impact point on the $[90/45/90/-45/90]2_s$ beam (2.59 mm x 27.91 mm x 228.6 mm) impacted with a 6.35 mm diameter steel ball at 46.65 m/sec.

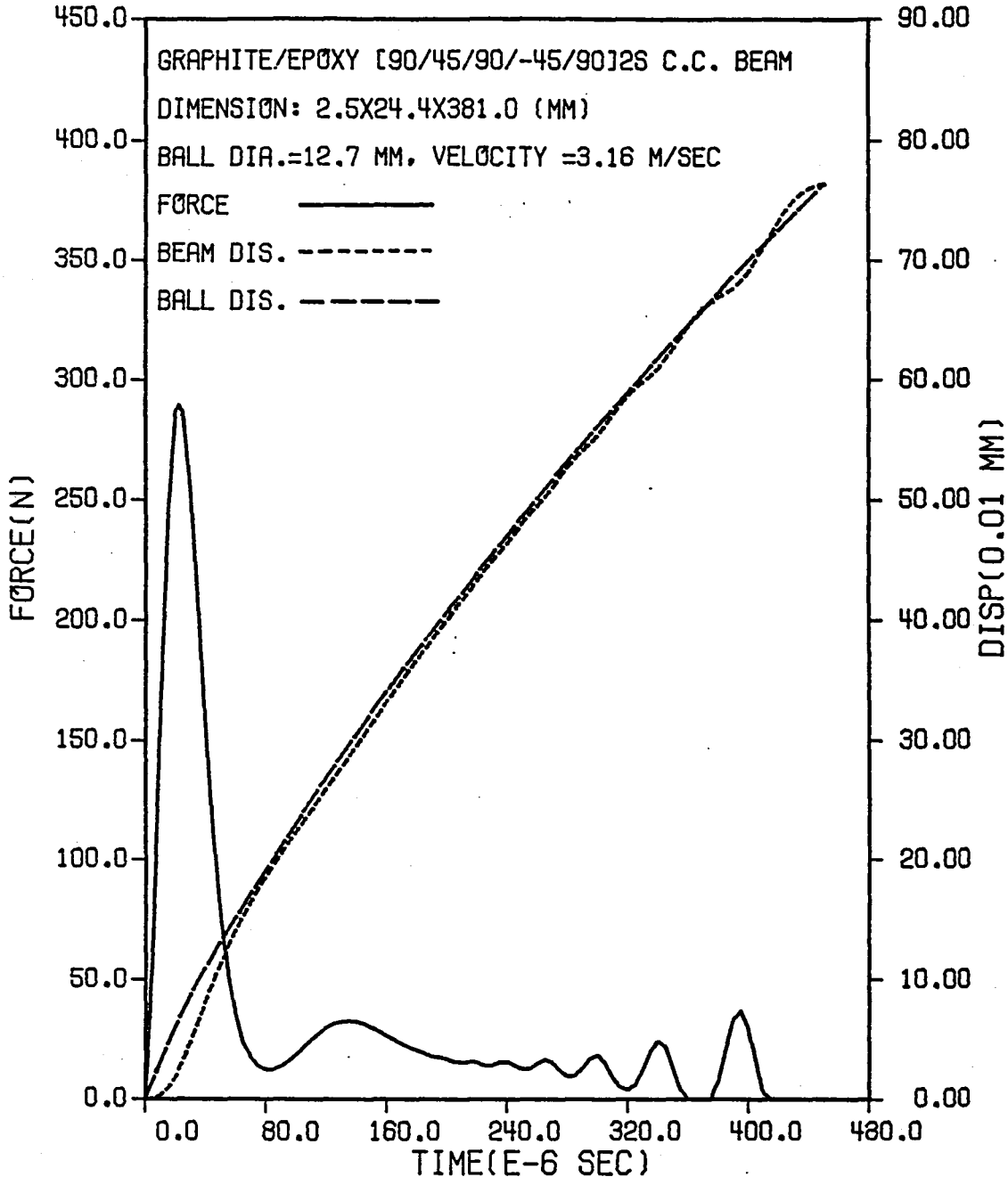

Fig. 4 Contact force and displacements of beam and ball for impact velocity 3.16 m/sec.

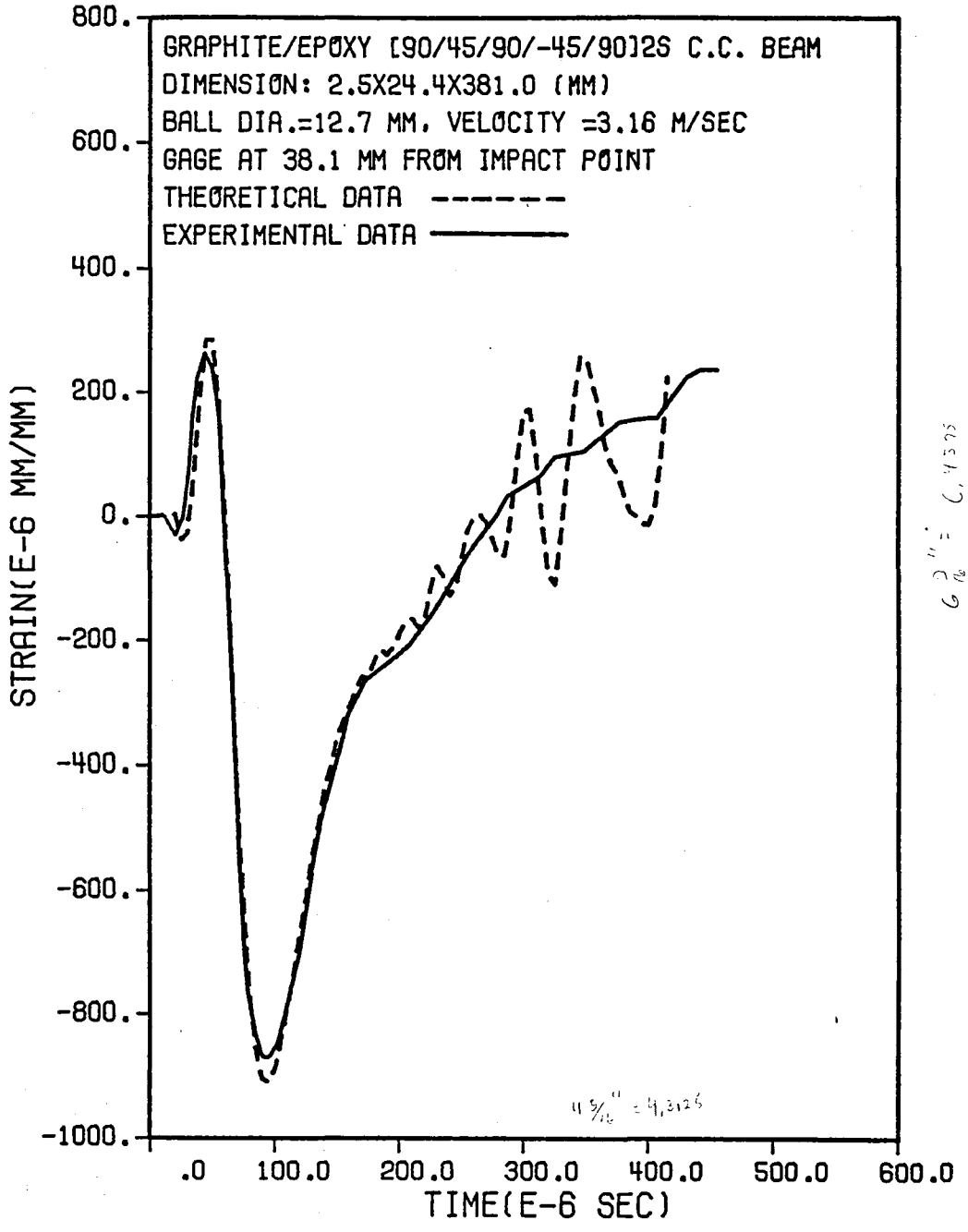

Fig. 5 Experimental and theoretical strain responses for a clamped-clamped $[90/45/90/-45/90]_{2s}$ beam at 38.1 mm from the impact point.

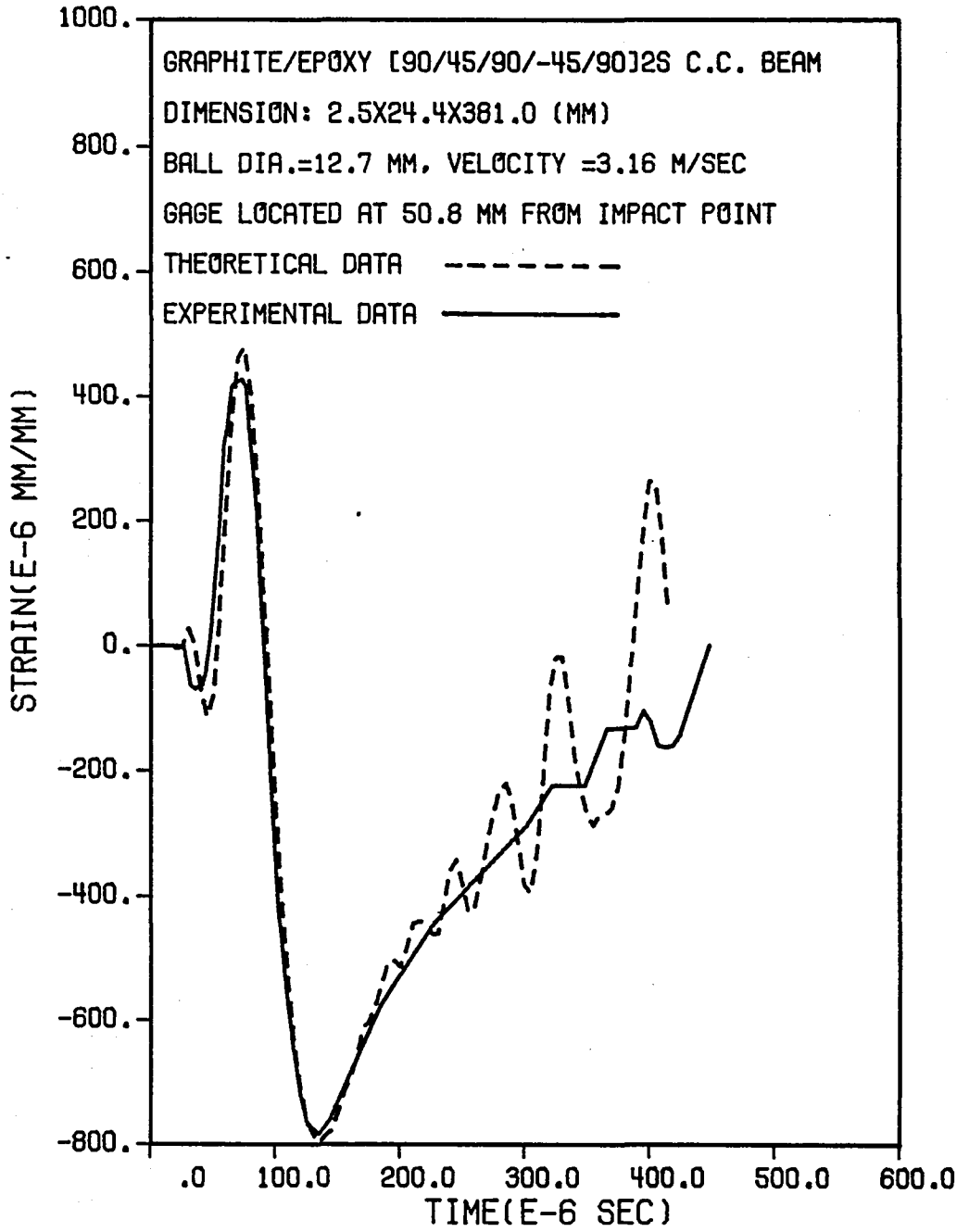

Fig. 6 Experimental and theoretical strain responses for a clamped-clamped $[90/45/90/-45/90]_{2s}$ beam at 50.8 mm from the impact point.

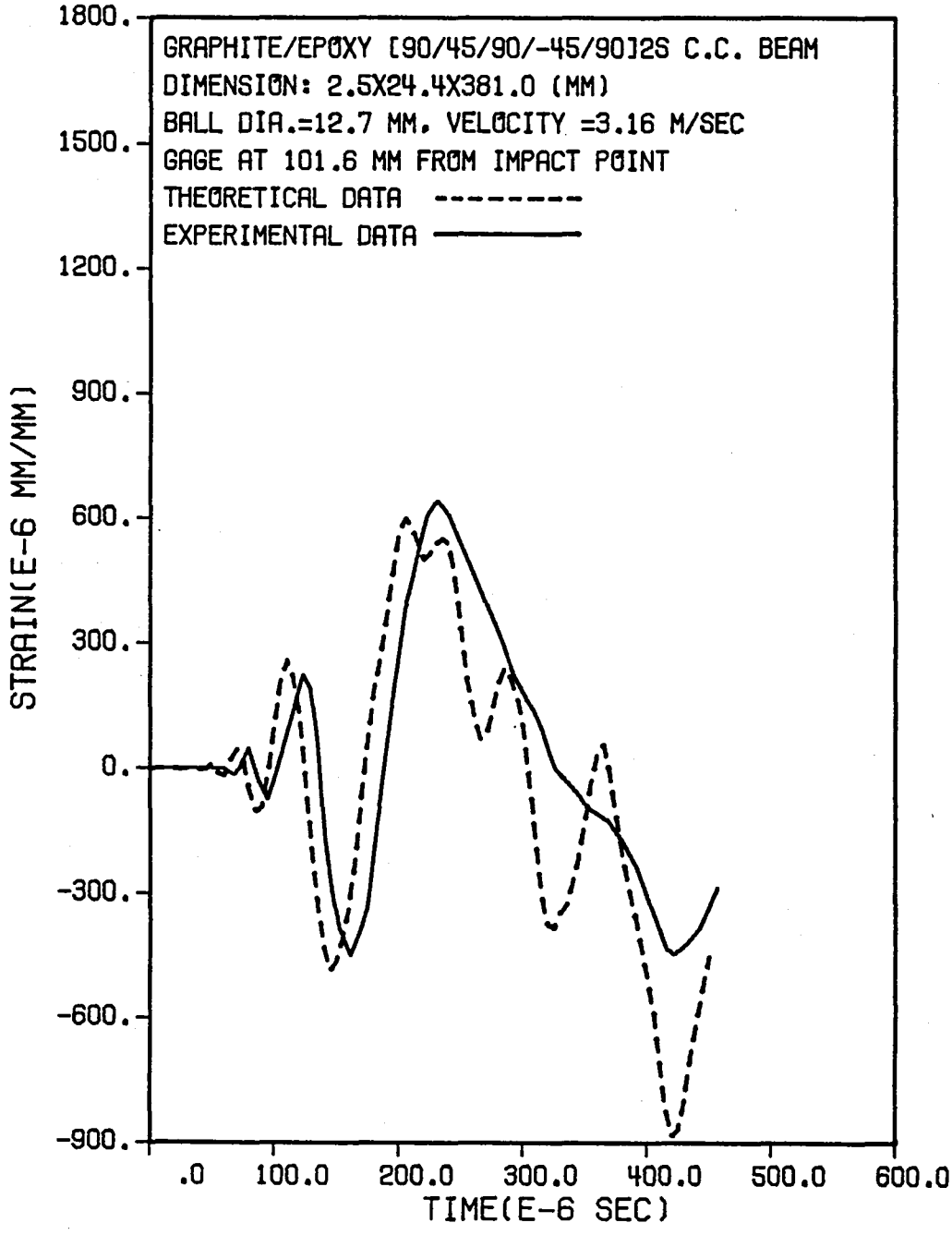

Fig. 7 Experimental and theoretical strain responses for a clamped-clamped $[90/45/90/-45/90]_{2s}$ beam at 101.6 mm from the impact point.

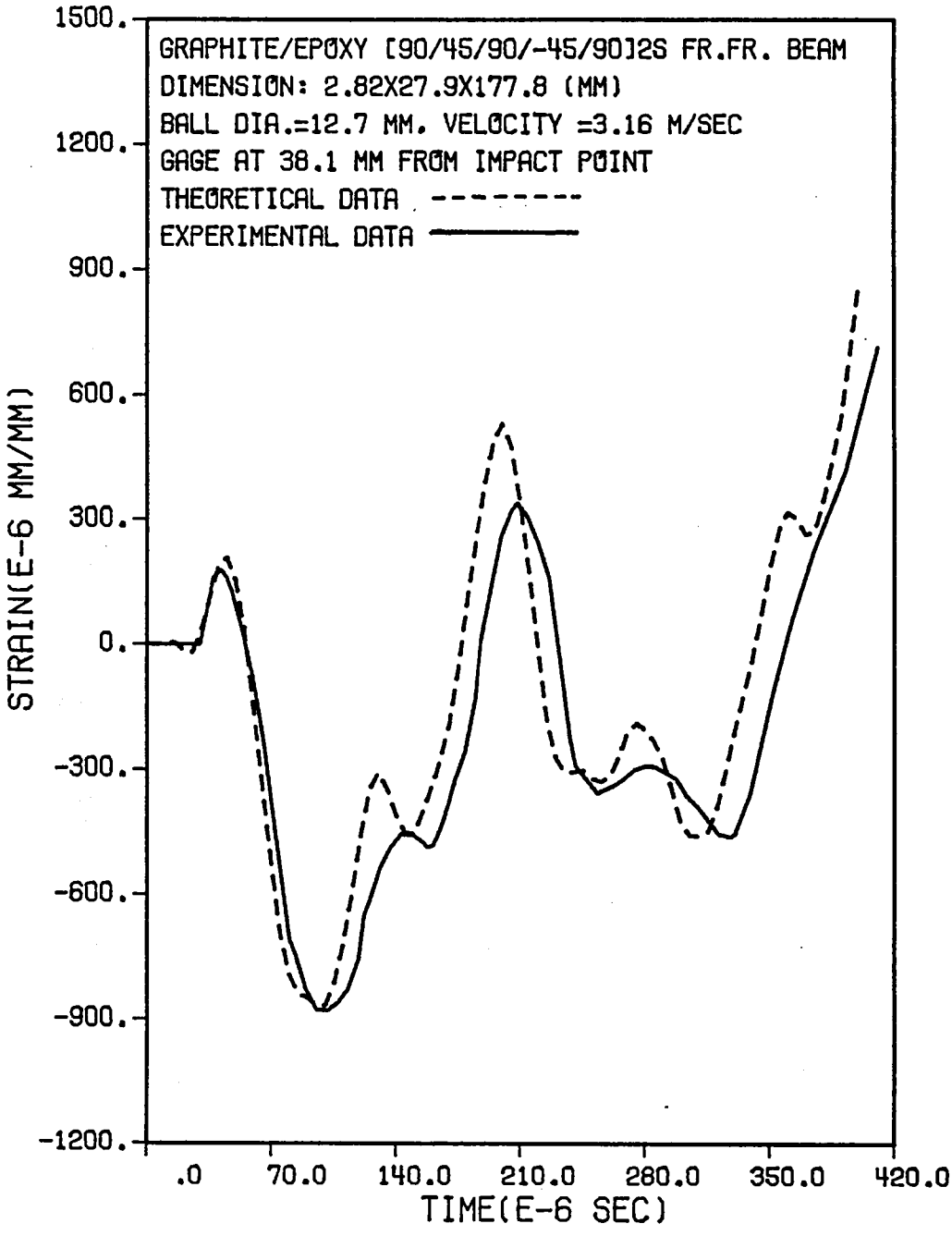

Fig. 8 Experimental and theoretical strain responses for a free-free $[90/45/90/-45/90]_{2s}$ beam at 38.1 mm from the impact point.

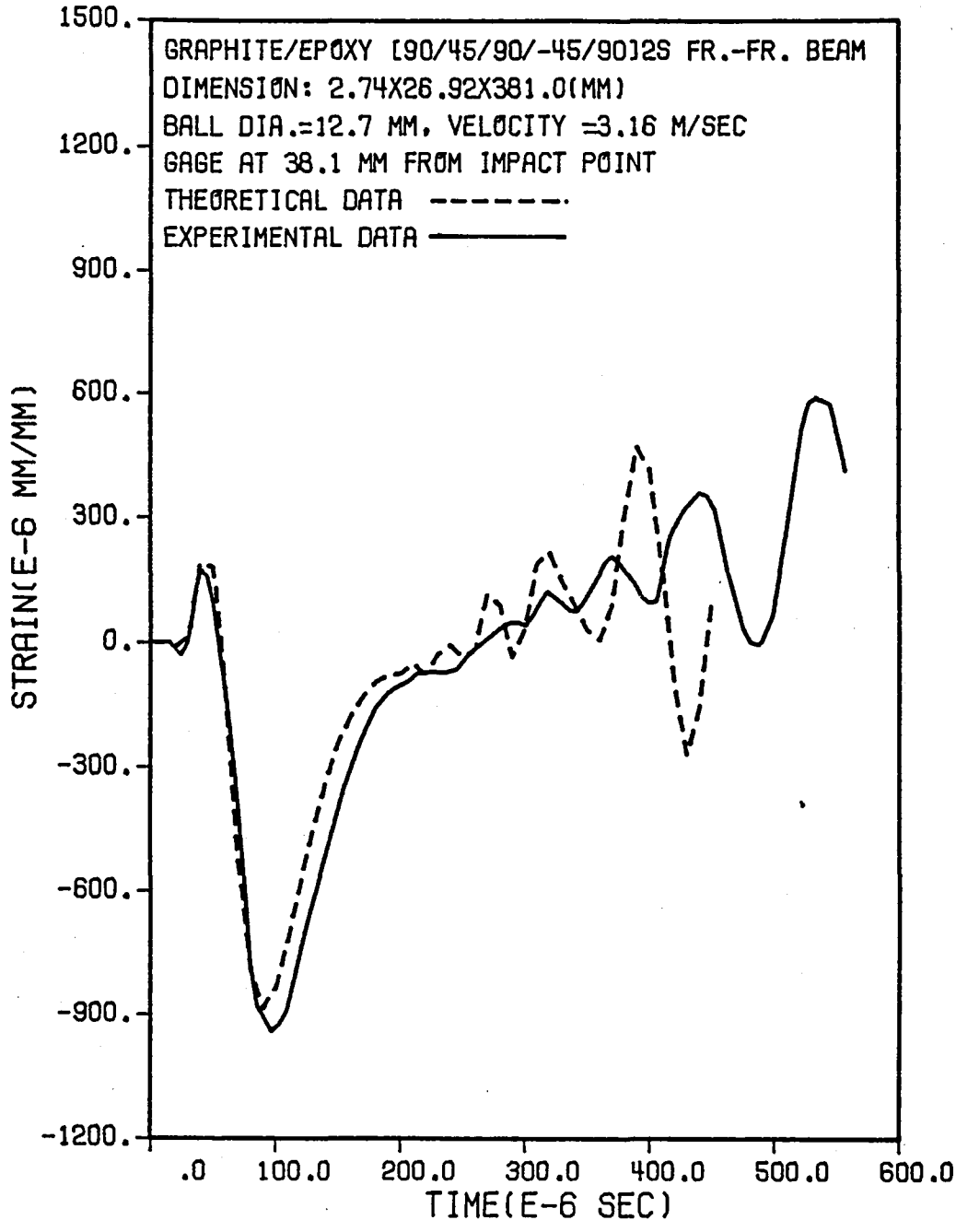

Fig. 9 Experimental and theoretical strain responses for a free-free $[90/45/90/-45/90]_{2s}$ beam at 38.1 mm from the impact point.

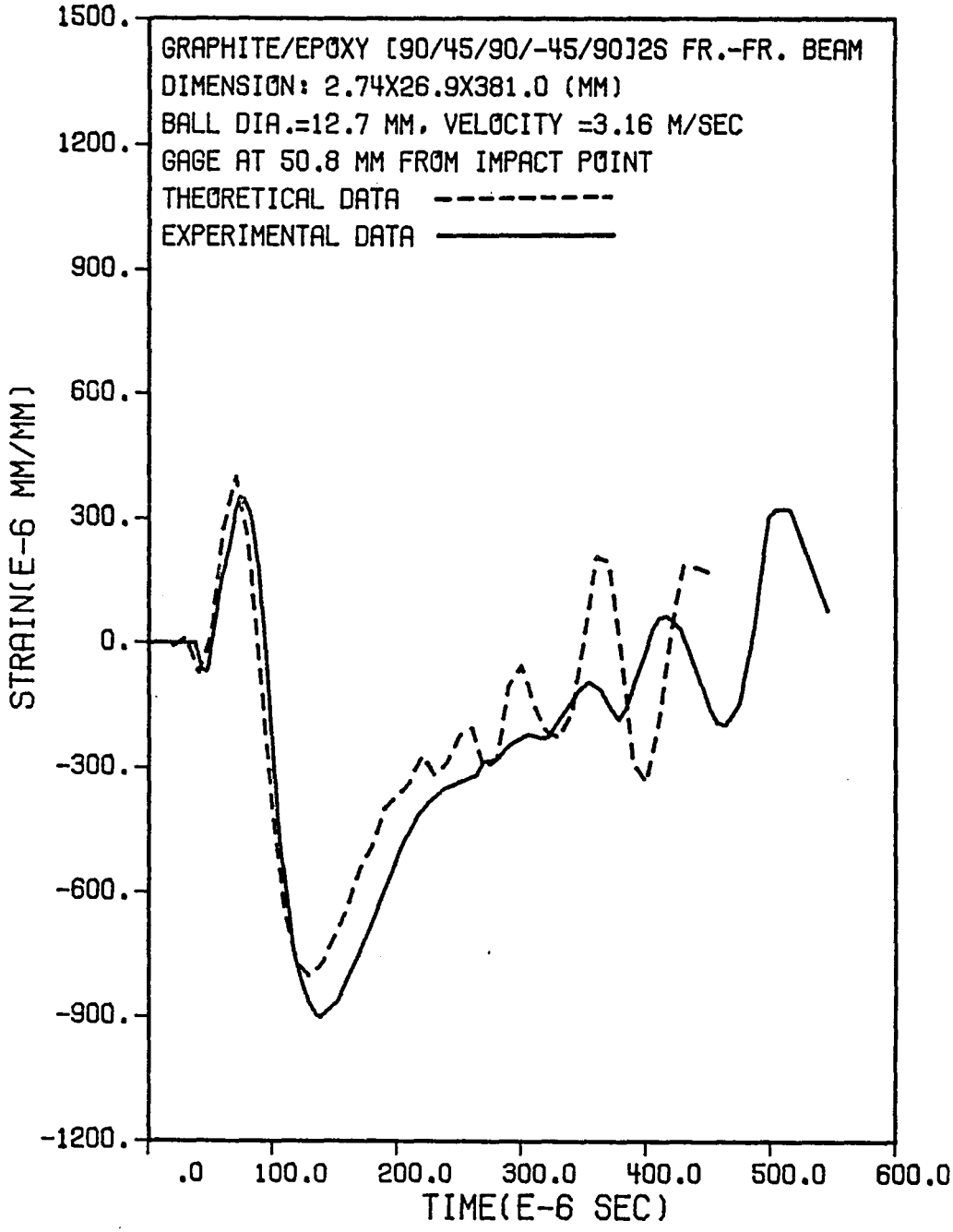

Fig. 10 Experimental and theoretical strain responses for a free-free $[90/45/90/-45/90]_{2s}$ beam at 50.8 mm from the impact point.

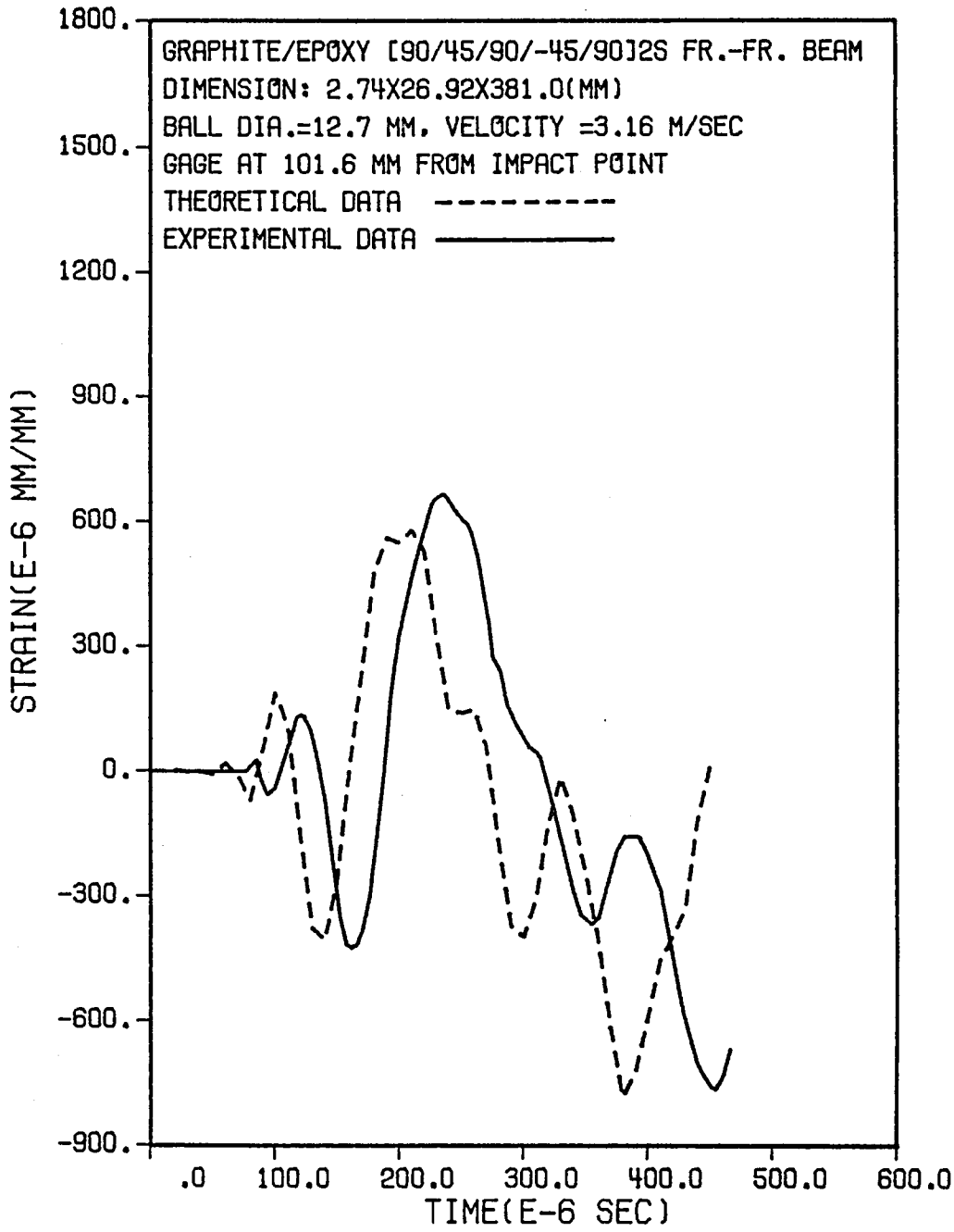

Fig. 11 Experimental and theoretical strain responses for a free-free $[90/45/90/-45/90]_{2s}$ beam at 101.6 mm from the impact point.

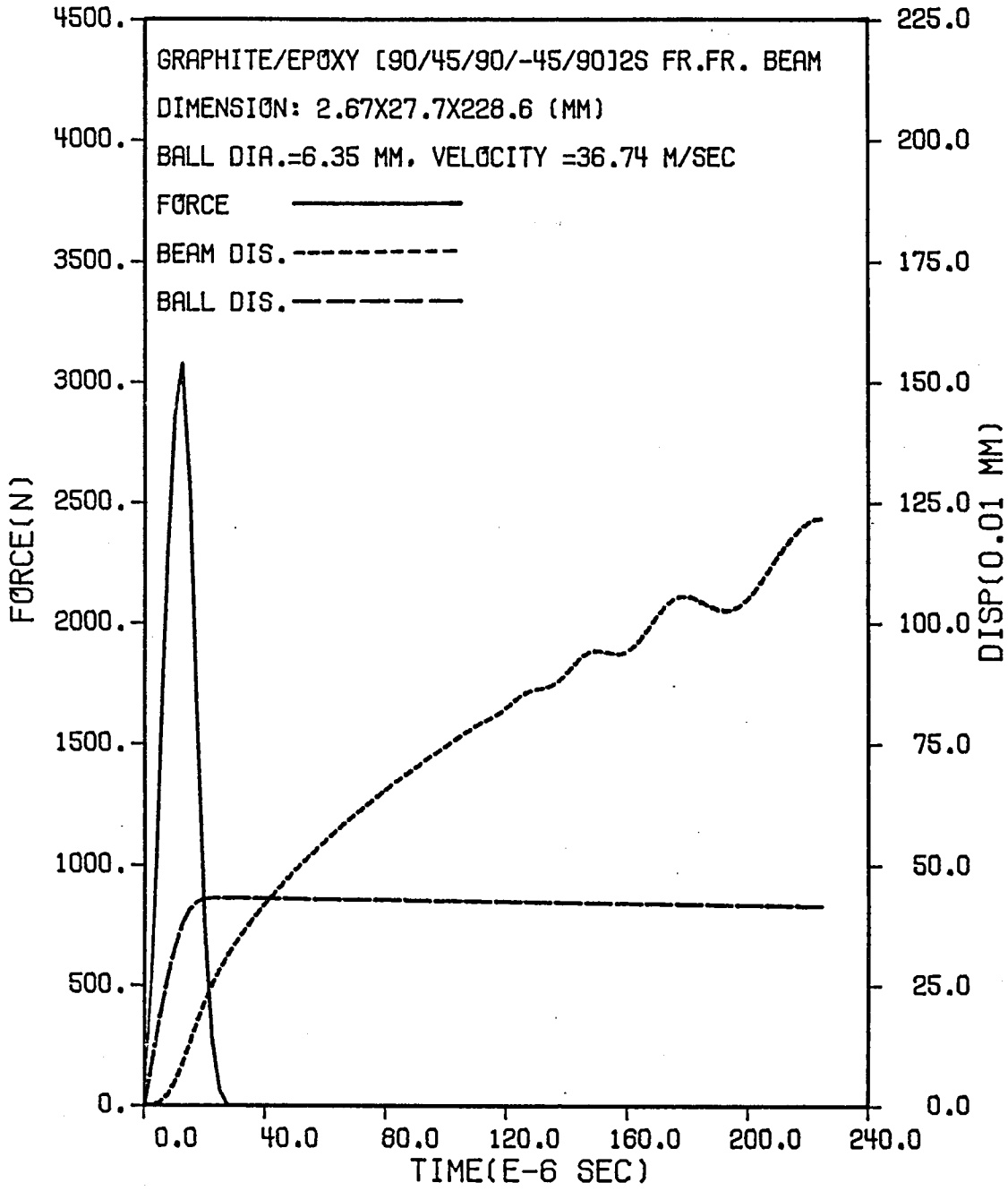

Fig. 12 Contact force and displacements of beam and ball for impact velocity 36.74 m/sec.

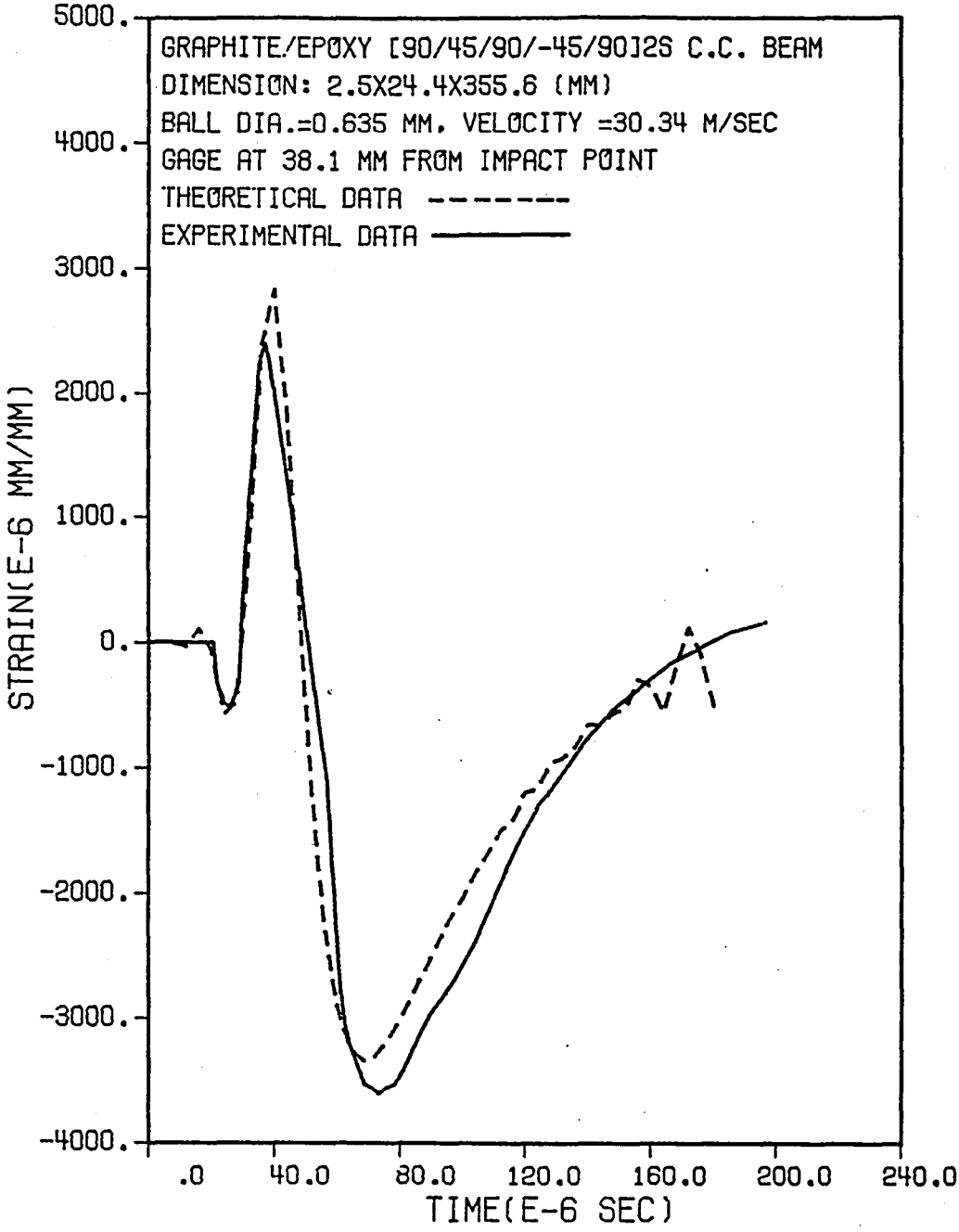

Fig. 13 Experimental and theoretical strain responses for a clamped-clamped $[90/45/90/-45/90]_{2s}$ beam at 38.1 mm from the impact point.

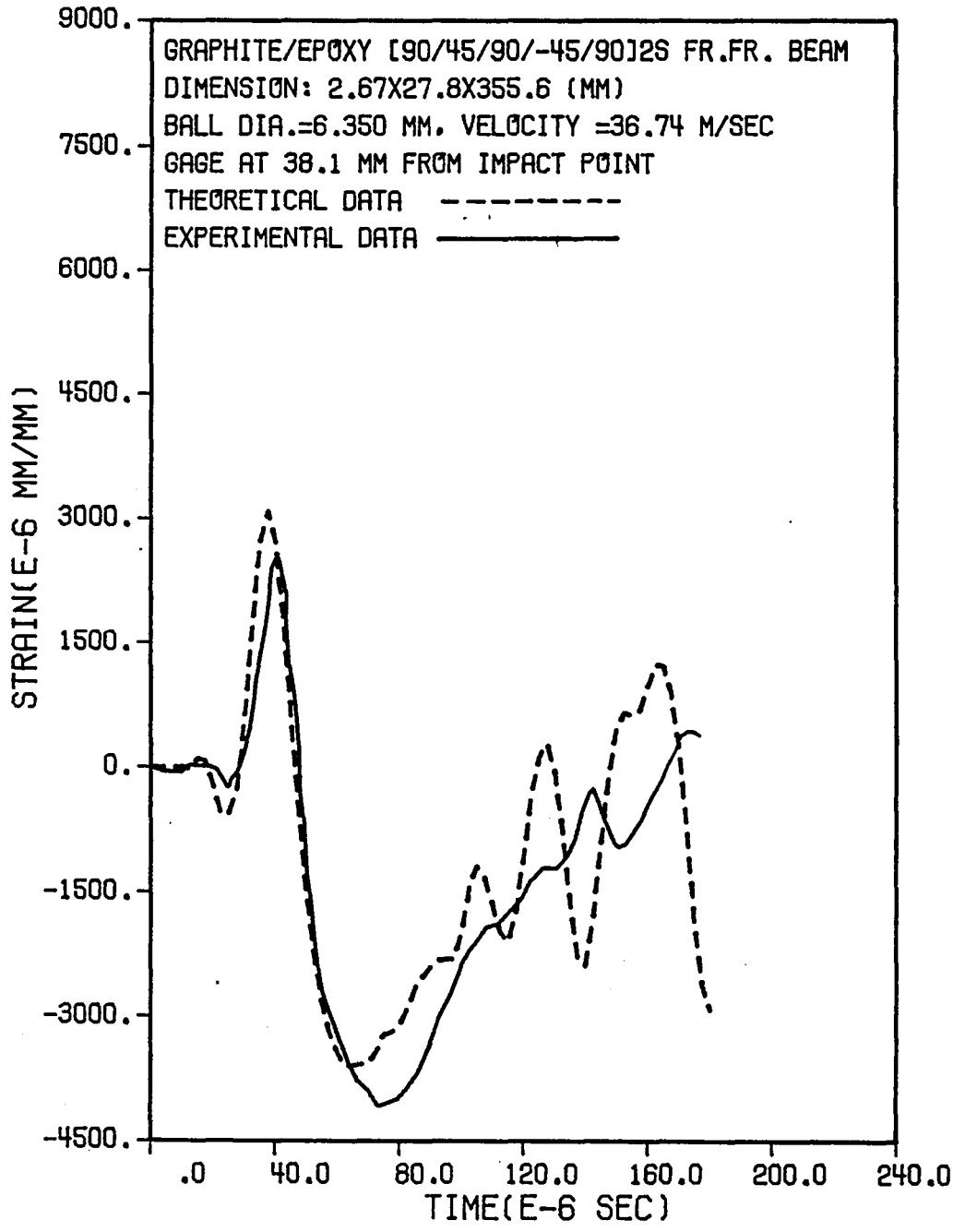

Fig. 14 Experimental and theoretical strain responses for a free-free $[90/45/90/-45/90]_{2s}$ beam at 38.1 mm from the impact point.

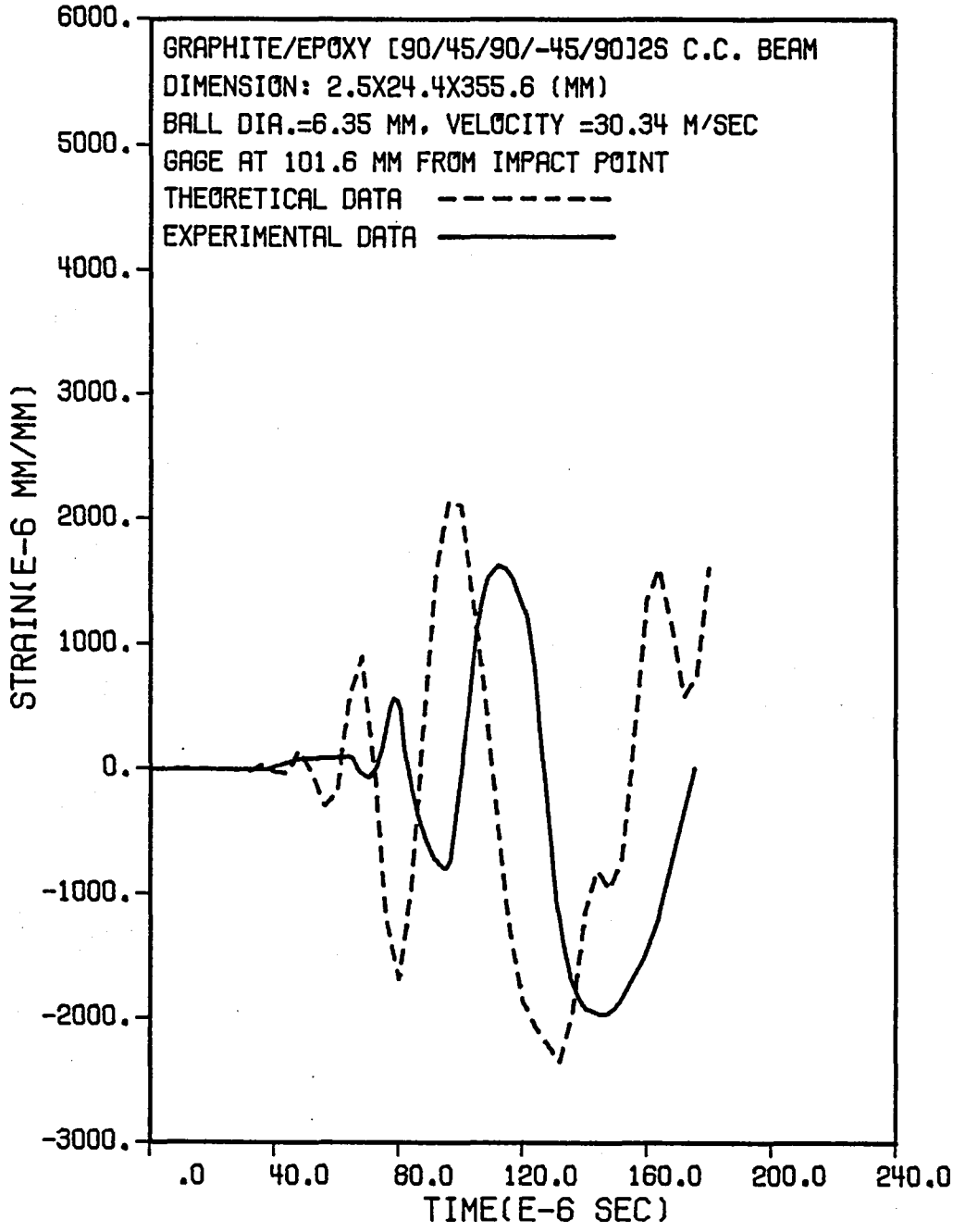

Fig. 15 Experimental and theoretical strain responses for a clamped-clamped $[90/45/90/-45/90]_{2s}$ beam at 101.6 mm from the impact point.

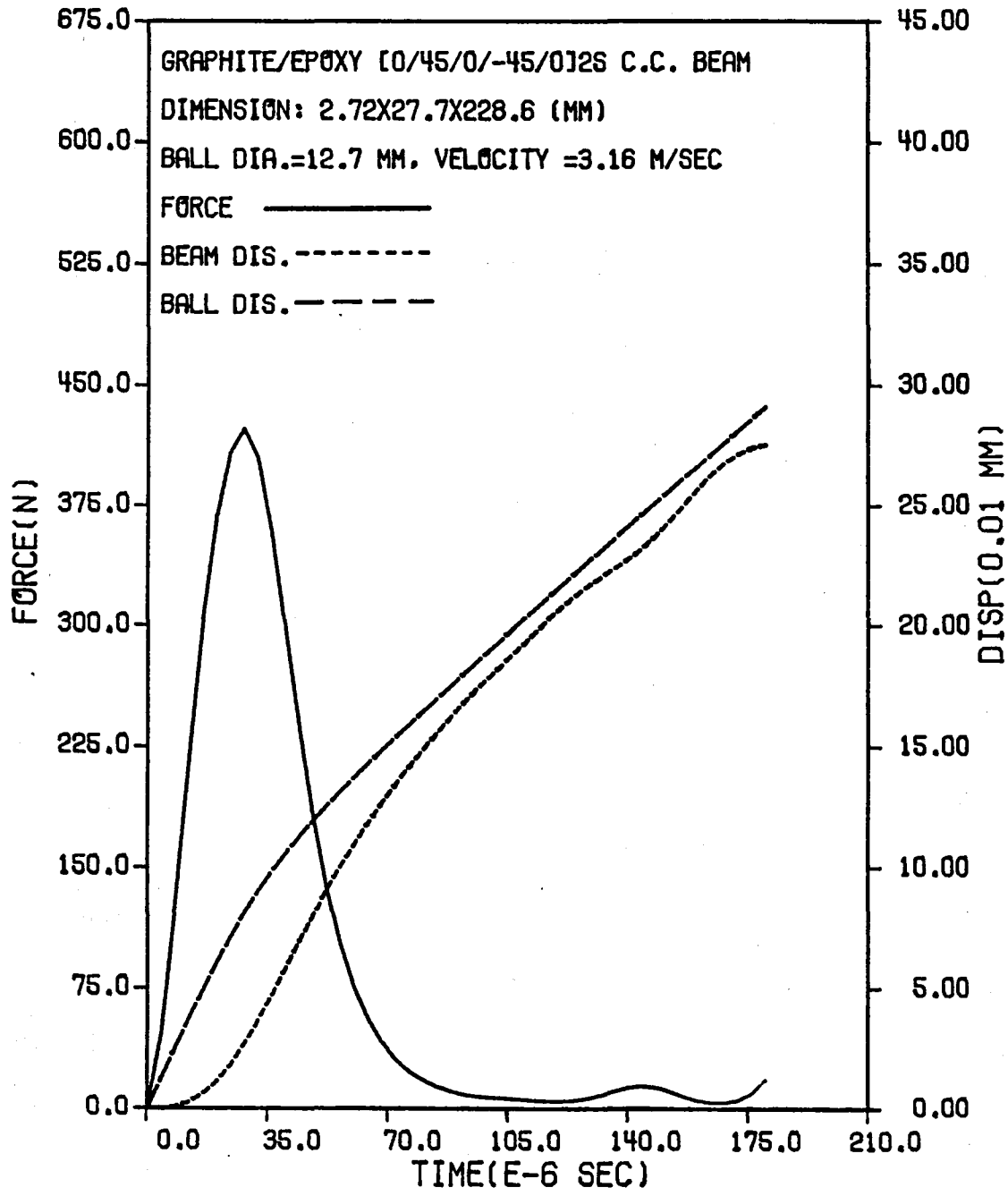

Fig. 16 Contact force and displacements of beam and ball for impact velocity 3.16 m/sec.

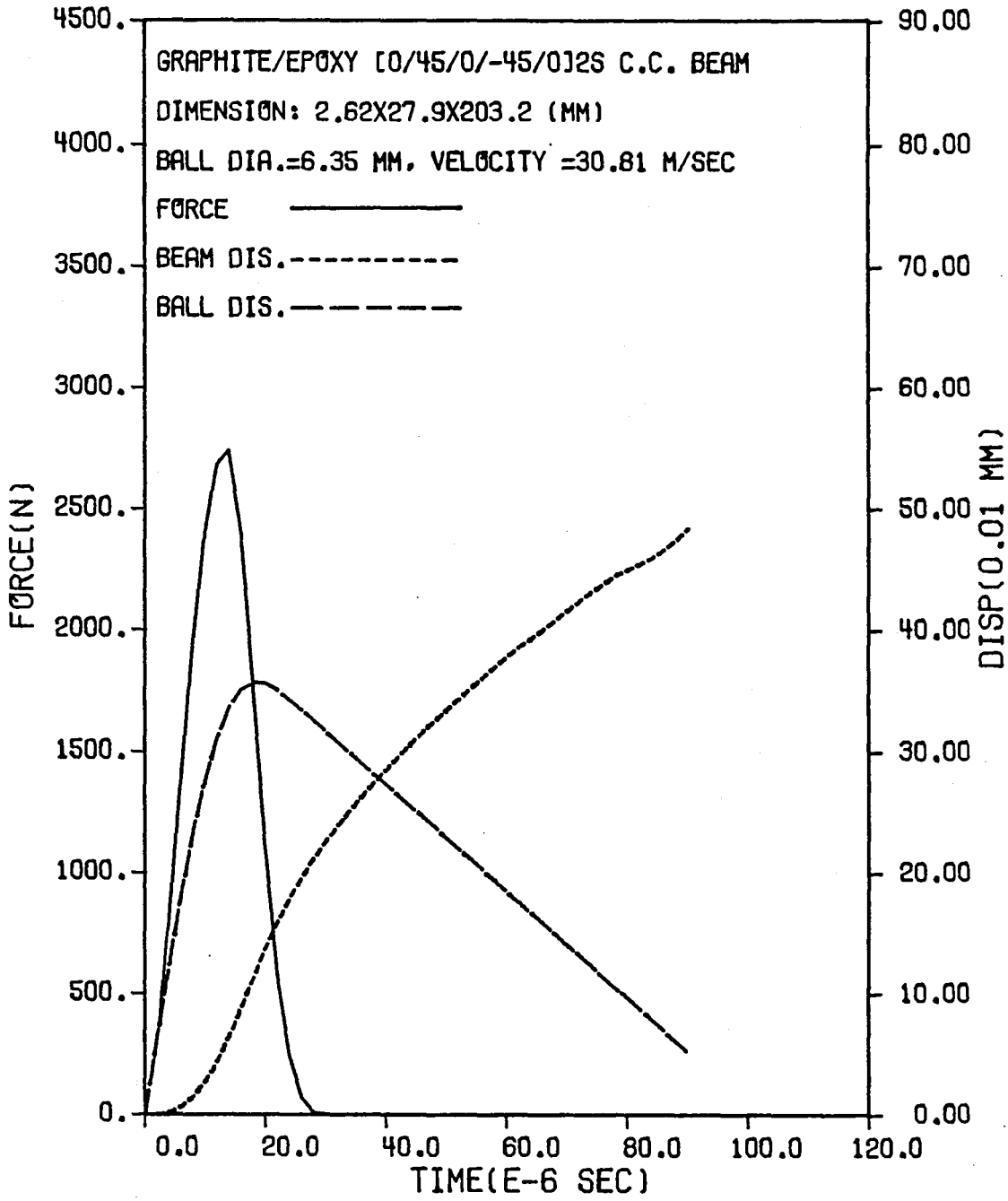

Fig. 17 Contact force and displacements of beam and ball for impact velocity 30.81 m/sec.

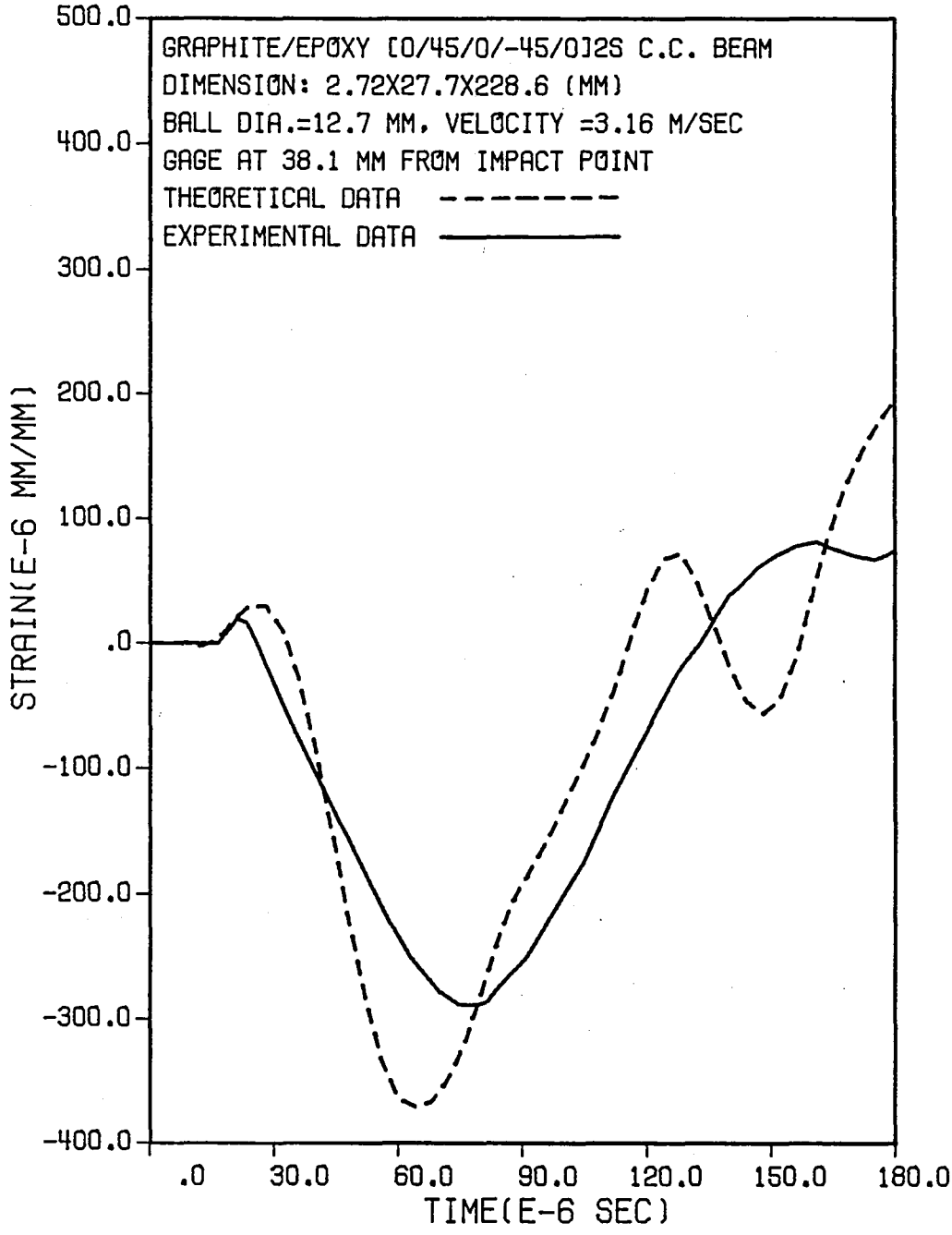

Fig. 18 Experimental and theoretical strain responses for a clamped-clamped $[0/45/0/-45/0]_{2s}$ beam at 38.1 mm from the impact point.

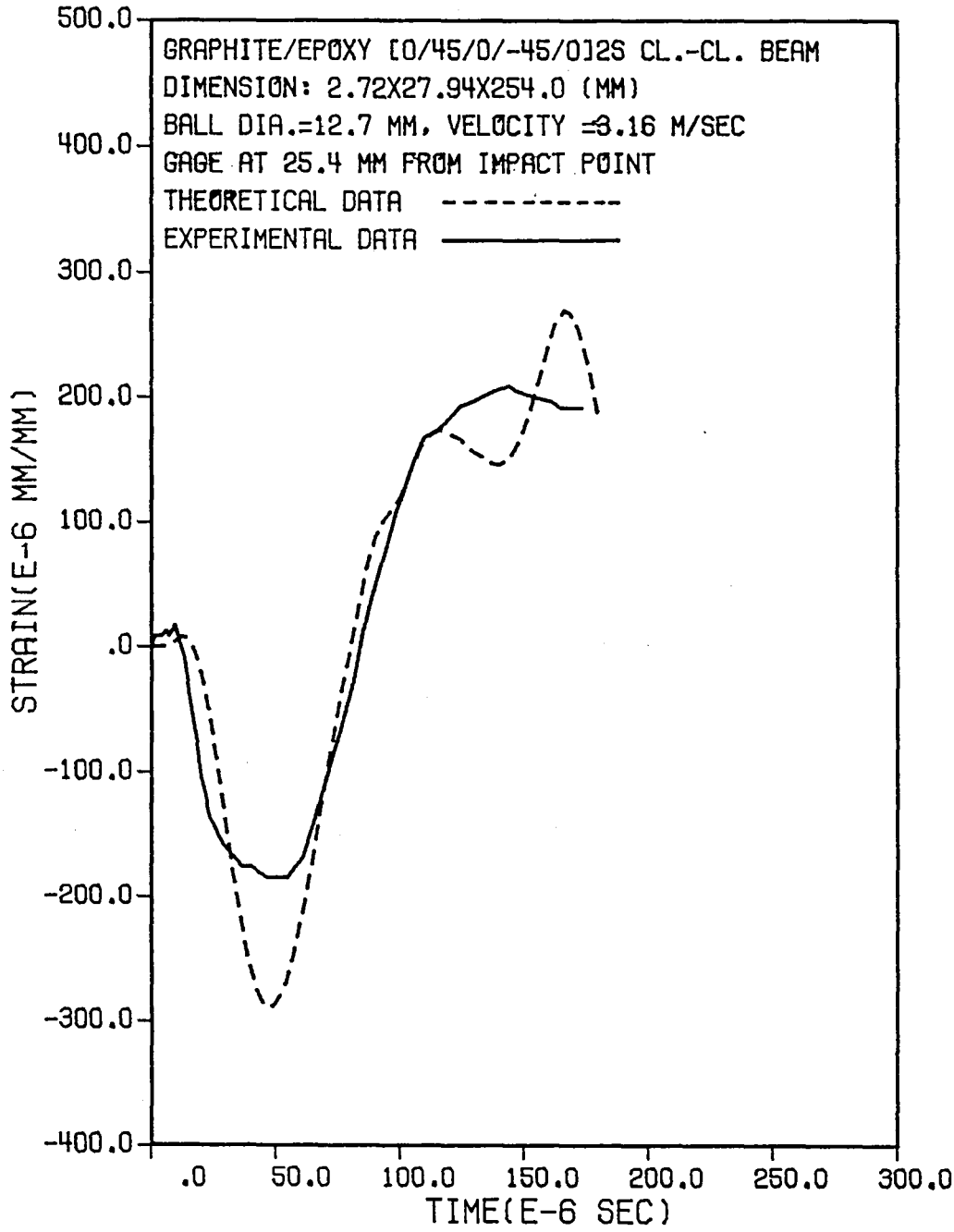

Fig. 19 Experimental and theoretical strain responses for a clamped-clamped $[0/45/0/-45/0]_{2s}$ beam at 25.4 mm from the impact point.

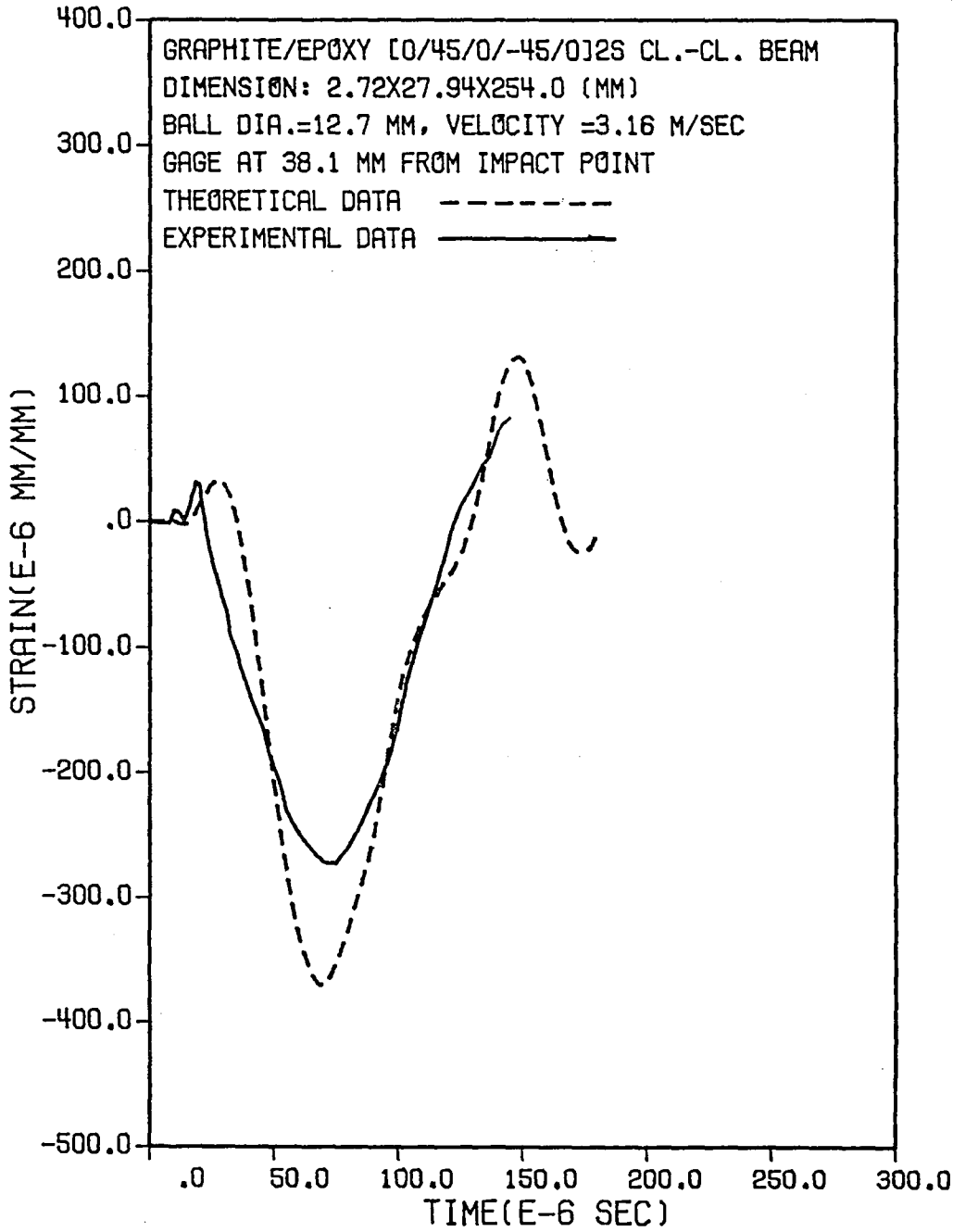

Fig. 20 Experimental and theoretical strain responses for a clamped-clamped $[0/45/0/-45/0]_{2s}$ beam at 38.1 mm from the impact point.

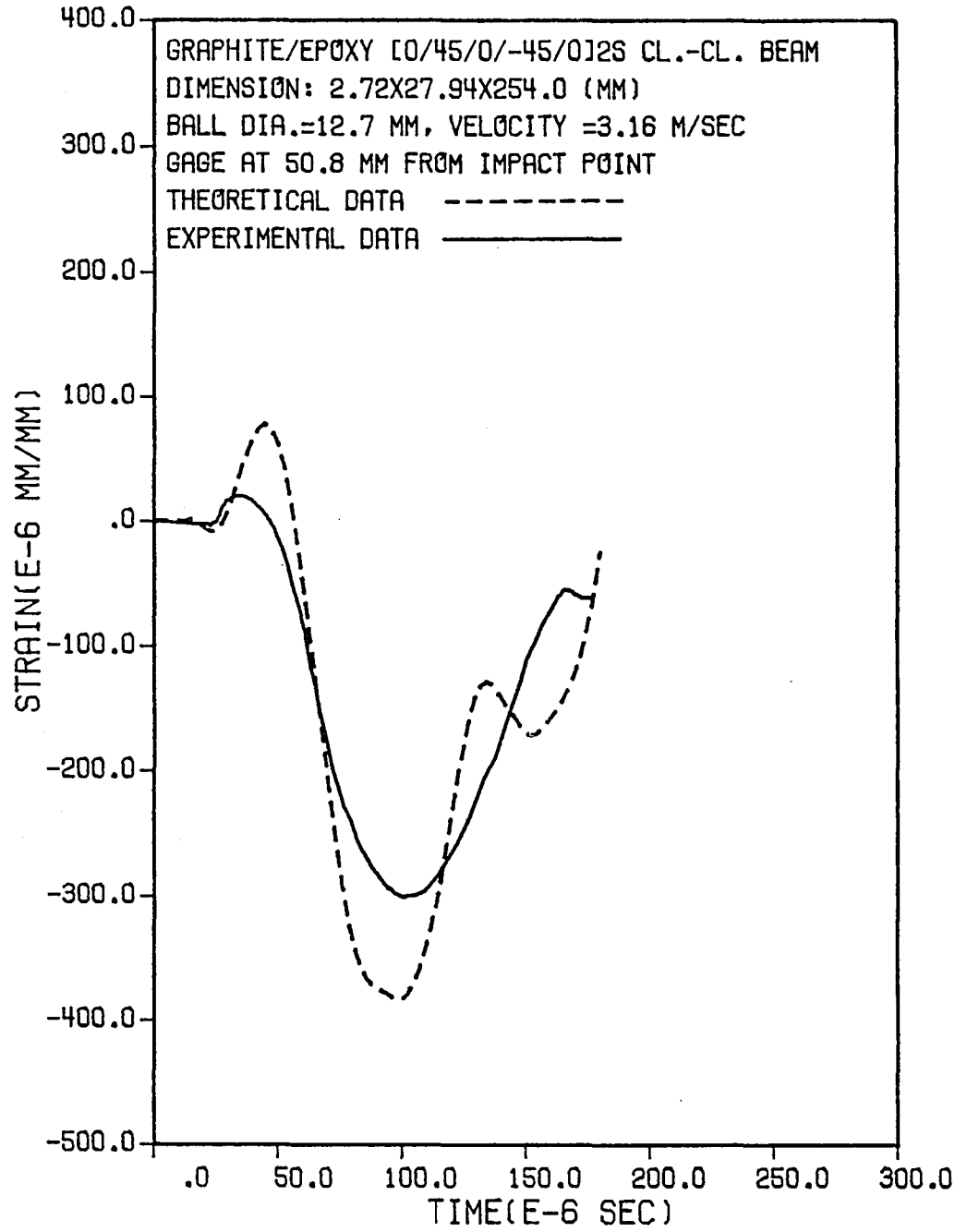

Fig. 21 Experimental and theoretical strain responses for a clamped-clamped $[0/45/0/-45/0]_{2s}$ beam at 50.8 mm from the impact point.

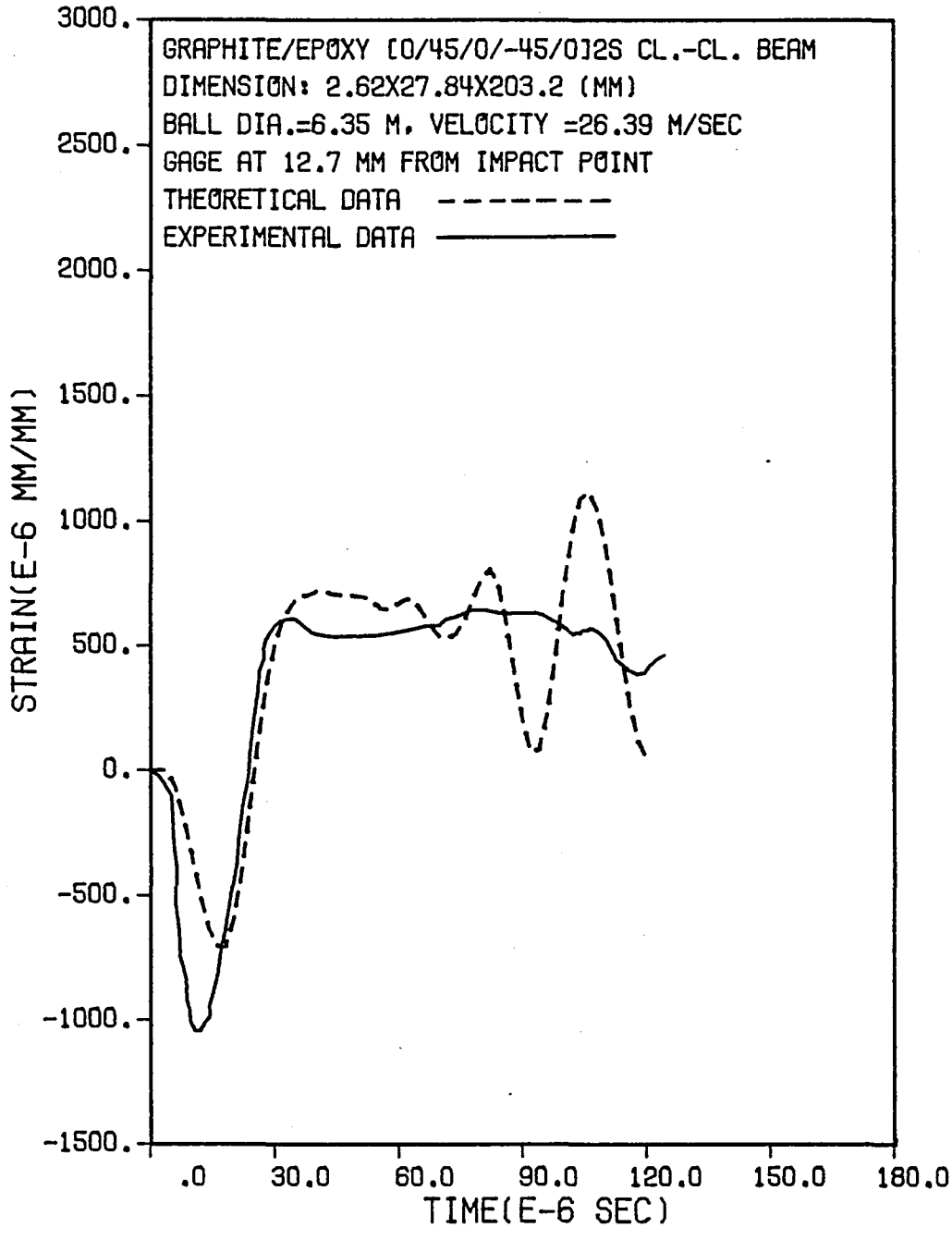

Fig. 22 Experimental and theoretical strain responses for a clamped-clamped $[0/45/0/-45/0]_{2s}$ beam at 12.7 mm from the impact point.

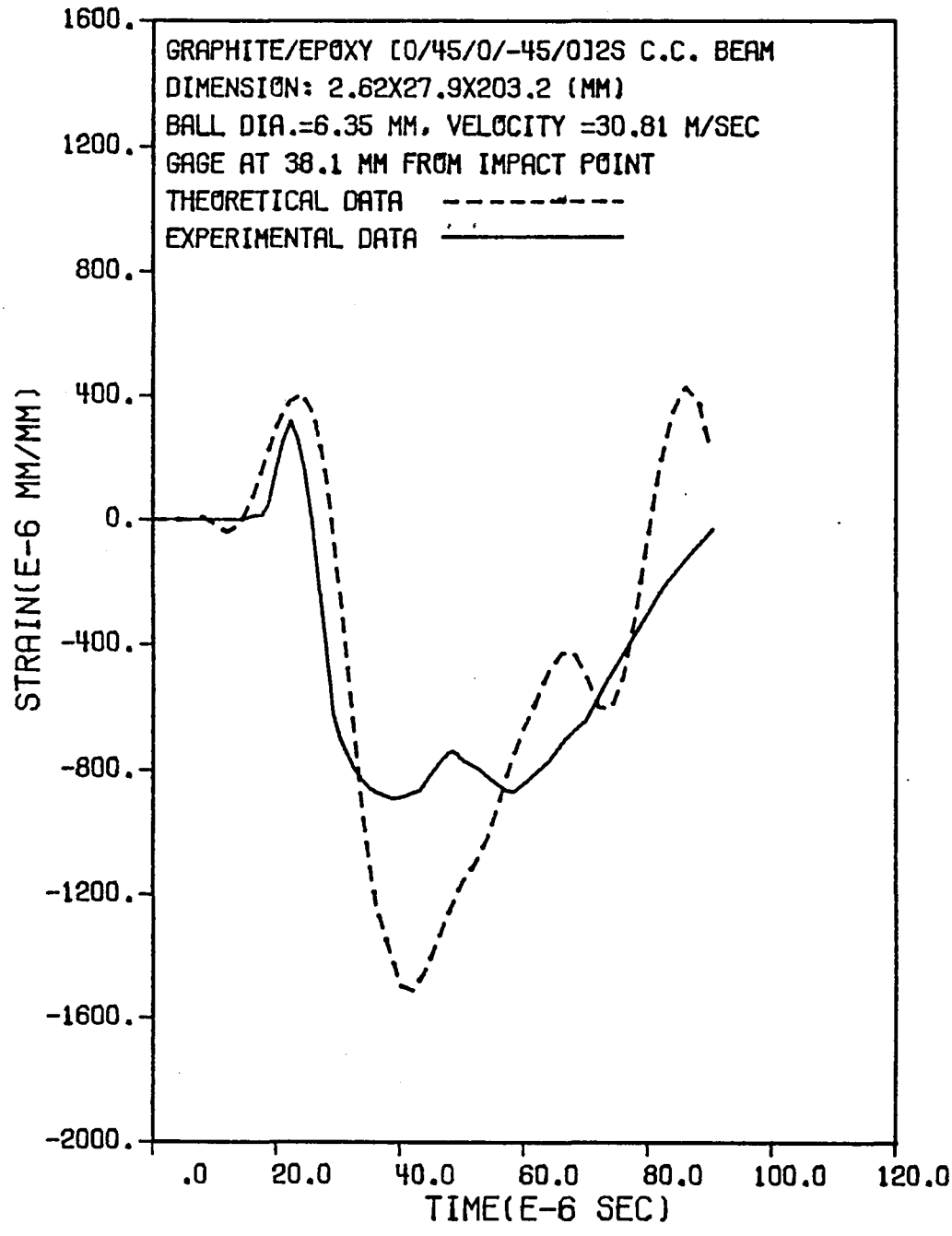

Fig. 23 Experimental and theoretical strain responses for a clamped-clamped $[0/45/0/-45/0]_{2s}$ beam at 38.1 mm from the impact point.

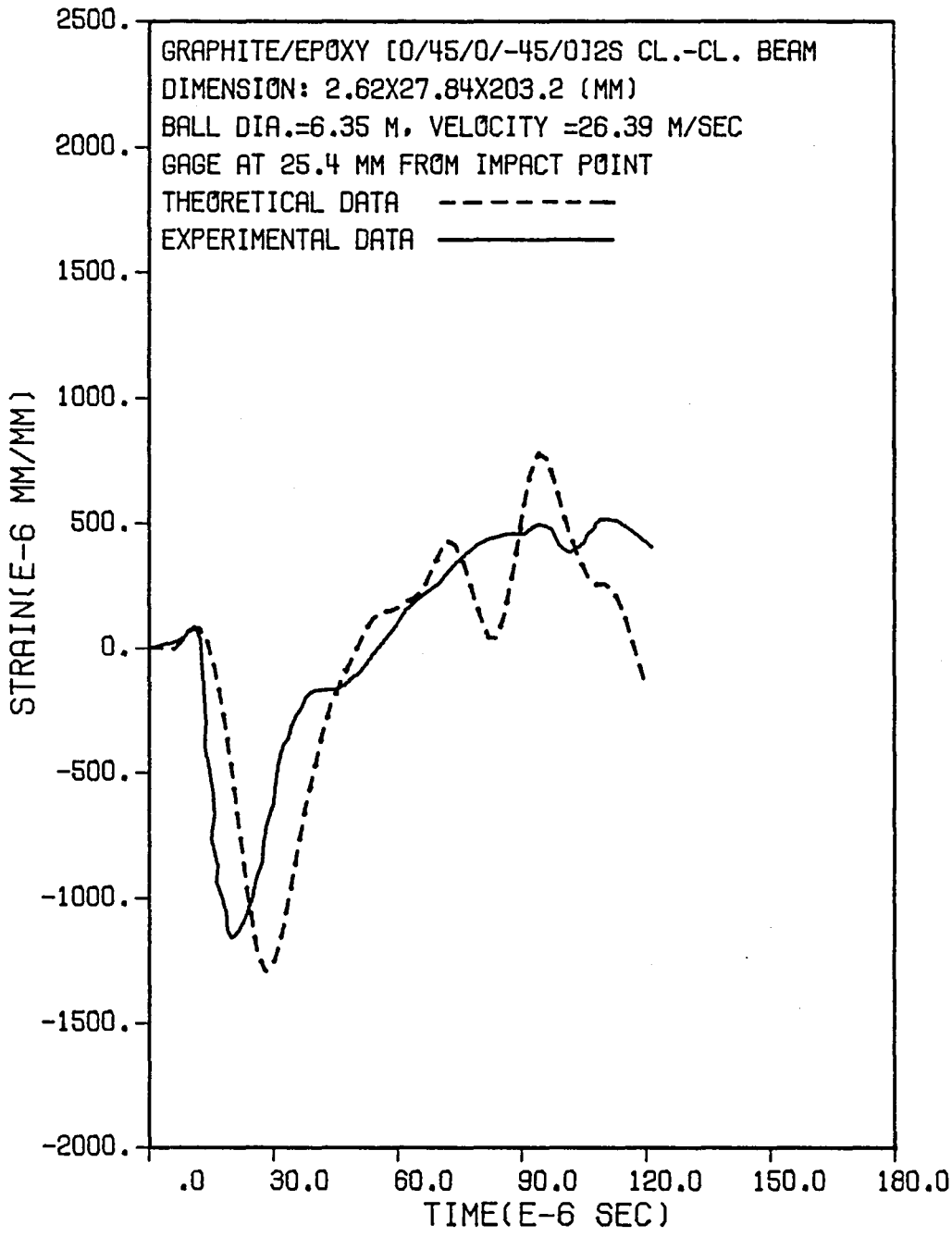

Fig. 24 Experimental and theoretical strain responses for a clamped-clamped $[0/45/0/-45/0]_{2s}$ beam at 25.4 mm from the impact point.

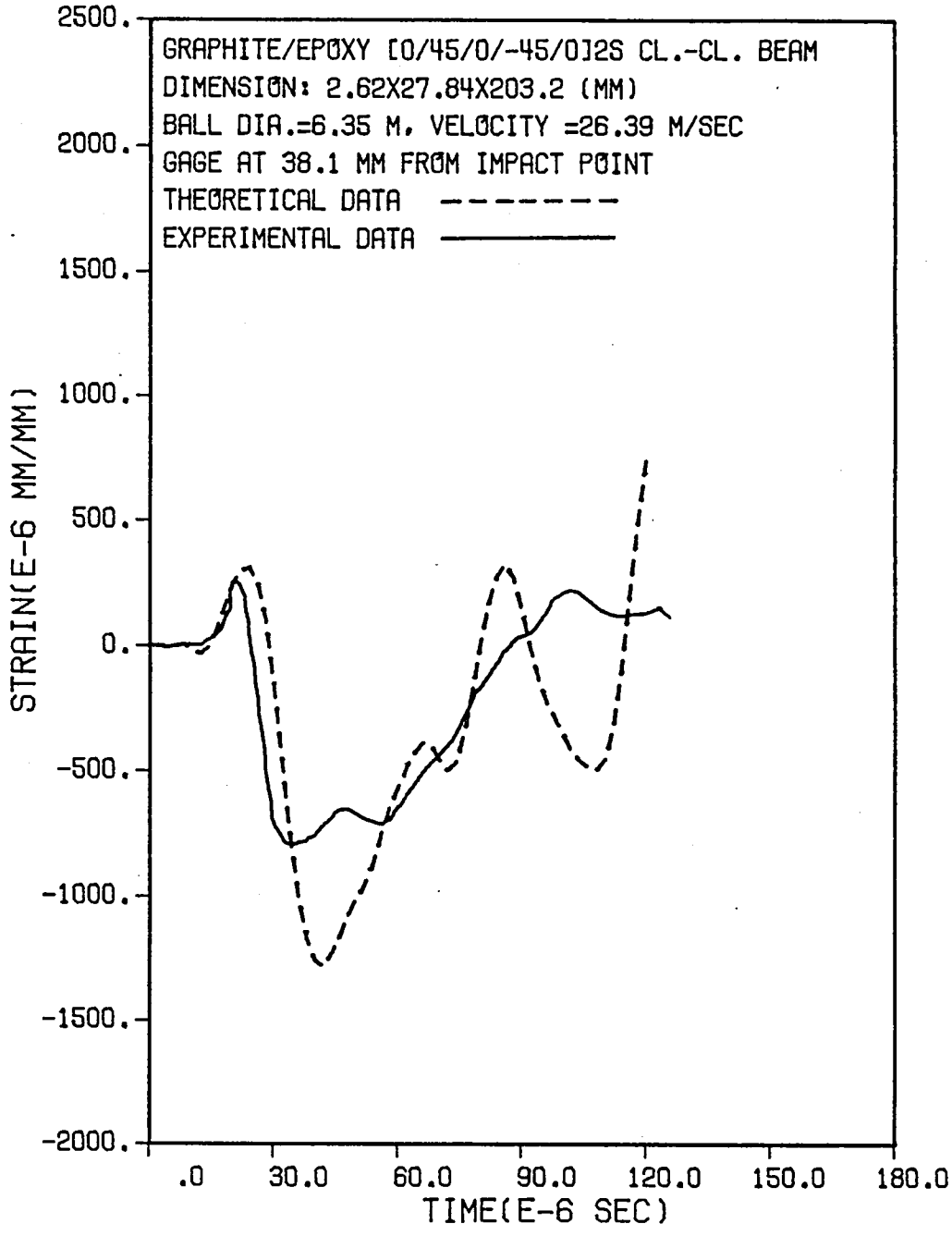

Fig. 25 Experimental and theoretical strain responses for a clamped-clamped $[0/45/0/-45/0]_{2s}$ beam at 38.1 mm from the impact point.

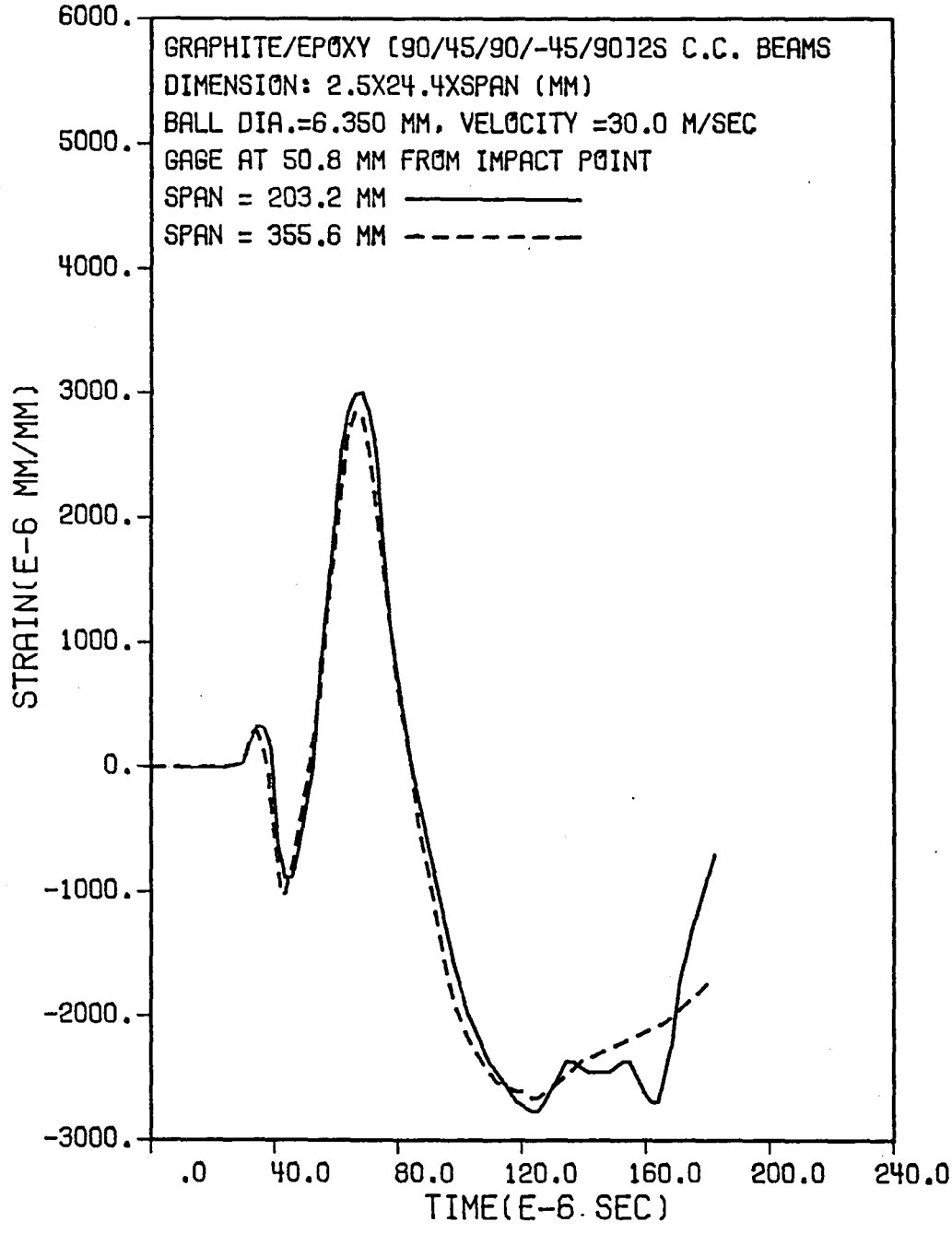

Fig. 26 Strain responses at 50.8 mm from the impact point for spans 203.2 mm and 355.6 mm.

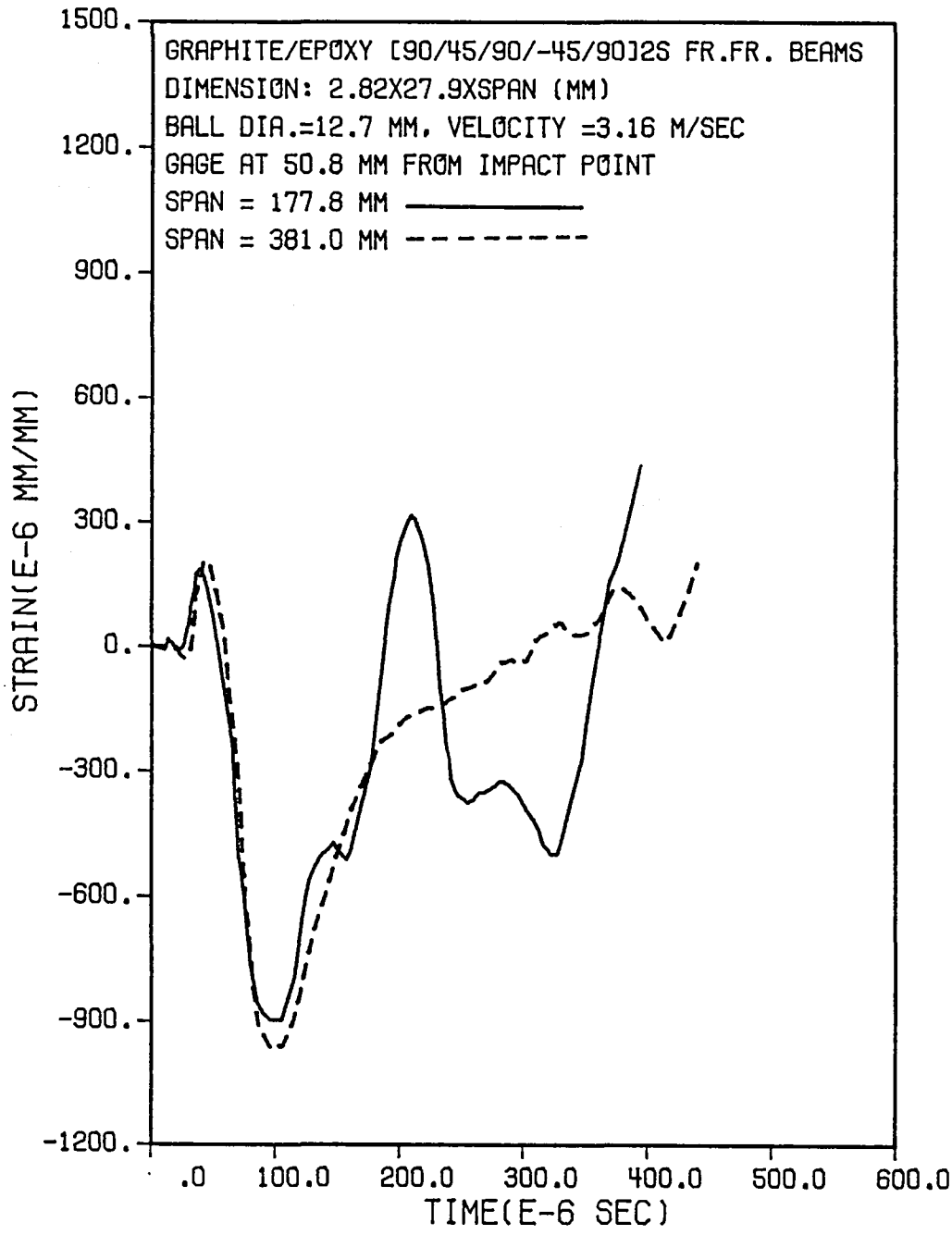

Fig. 27 Strain responses at 38.1 mm from the impact point for spans 177.8 mm and 381.0 mm.

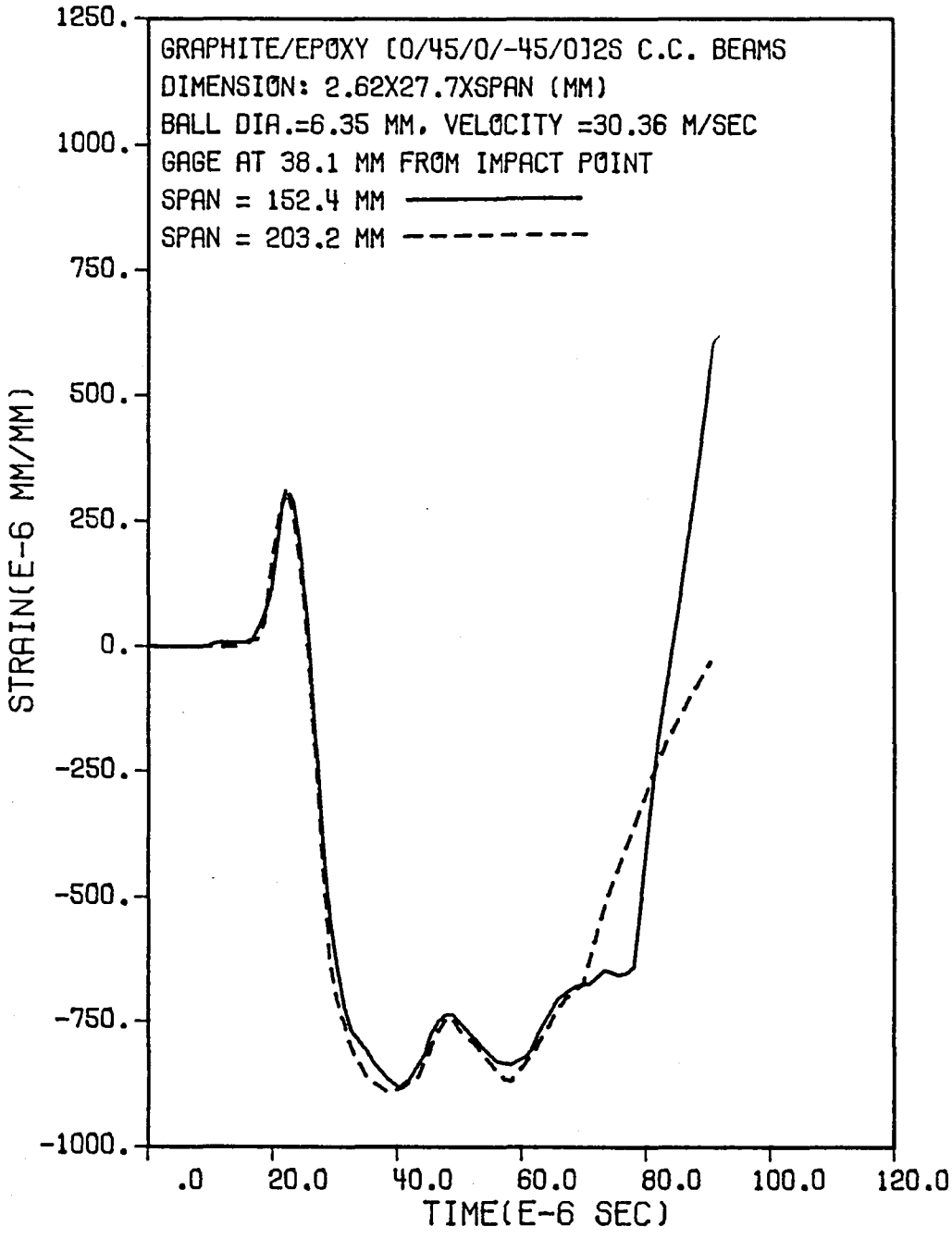

Fig. 28 Strain responses at 38.1 mm from the impact point for spans 152.4 mm and 203.2 mm.

TOPICAL REPORT

NSG-3185

DYNAMIC RESPONSES OF A GRAPHITE/EPOXY LAMINATES BEAM TO IMPACT OF ELASTIC SPHERES

NASA CR-165461

Advanced Research Projects Agency
Washington DC 20525
Attn: Library

Advanced Technology Center, Inc.
LTV Aerospace Corporation
P.O. Box 6144
Dallas, TX 75222
Attn: D. H. Petersen
W. J. Renton

Air Force Flight Dynamics Laboratory
Wright-Patterson Air Force Base, OH 45433
Attn: E. E. Baily
G. P. Sendeckyj (FBC)
R. S. Sandhu

Air Force Materials Laboratory
Wright-Patterson Air Force Base, OH 45433
Attn: H. S. Schwartz (LN)
T. J. Reinhart (MBC)
G. P. Peterson (LC)
E. J. Morrisey (LAE)
S. W. Tsai (MBM)
N. J. Pagano
J. M. Whitney (MBM)

Air Force Office of Scientific Research
Washington DC 20333
Attn: J. F. Masi (SREP)

Air Force Office of Scientific Research
1400 Wilson Blvd.
Arlington, VA 22209

AFOSR/NA
Bolling AFB, DC 20332
Attn: A. K. Amos

Air Force Rocket Propulsion Laboratory
Edwards, CA 93523
Attn: Library

Babcock & Wilcox Company
Advanced Composites Department
P.O. Box 419
Alliance, Ohio 44601
Attn: P. M. Leopold

Bell Helicopter Company
P.O. Box 482
Ft. Worth, TX 76101
Attn: H. Zinberg

The Boeing Company
P. O. Box 3999
Seattle, WA 98124
Attn: J. T. Hoggatt, MS. 88-33
T. R. Porter

The Boeing Company
Vertol Division
Morton, PA 19070
Attn: E. C. Durchlaub

Battelle Memorial Institute
Columbus Laboratories
505 King Avenue
Columbus, OH 43201
Attn: L. E. Hulbert

Bendix Advanced Technology Center
9140 Old Annapolis Rd/Md. 108
Columbia, MD 21045
Attn: O. Hayden Griffin

Brunswick Corporation
Defense Products Division
P. O. Box 4594
43000 Industrial Avenue
Lincoln, NE 68504
Attn: R. Morse

Celanese Research Company
86 Morris Ave.
Summit, NJ 07901
Attn: H. S. Kliger

Commander
Natick Laboratories
U. S. Army
Natick, MA 01762
Attn: Library

Commander
Naval Air Systems Command
U. S. Navy Department
Washington DC 20360
Attn: M. Stander, AIR-43032D

Commander
Naval Ordnance Systems Command
U.S. Navy Department
Washington DC 20360
Attn: B. Drimmer, ORD-033
M. Kinna, ORD-033A

Cornell University
Dept. Theoretical & Applied Mech.
Thurston Hall
Ithaca, NY 14853
Attn: S. L. Phoenix

Defense Metals Information Center
Battelle Memorial Institute
Columbus Laboratories
505 King Avenue
Columbus, OH 43201

Department of the Army
U.S. Army Aviation Materials Laboratory
Ft. Eustis, VA 23604
Attn: I. E. Figge, Sr.
Library

Department of the Army
U.S. Army Aviation Systems Command
P.O. Box 209
St. Louis, MO 63166
Attn: R. Vollmer, AMSAV-A-UE

Department of the Army
Plastics Technical Evaluation Center
Picatinny Arsenal
Dover, NJ 07801
Attn: H. E. Pebly, Jr.

Department of the Army
Watervliet Arsenal
Watervliet, NY 12189
Attn: G. D'Andrea

Department of the Army
Watertown Arsenal
Watertown, MA 02172
Attn: A. Thomas

Department of the Army
Redstone Arsenal
Huntsville, AL 35809
Attn: R. J. Thompson, AMSMI-RSS

Department of the Navy
Naval Ordnance Laboratory
White Oak
Silver Spring, MD 20910
Attn: R. Simon

Department of the Navy
U.S. Naval Ship R&D Laboratory
Annapolis, MD 21402
Attn: C. Hersner, Code 2724

Director
Deep Submergence Systems Project
6900 Wisconsin Avenue
Washington DC 20015
Attn: H. Bernstein, DSSP-221

Director
Naval Research Laboratory
Washington DC 20390
Attn: Code 8430
I. Wolock, Code 8433

Drexel University
32nd and Chestnut Streets
Philadelphia, PA 19104
Attn: P. C. Chou

E. I. DuPont DeNemours & Co.
DuPont Experimental Station
Wilmington, DE 19898
Attn: D. L. G. Sturgeon

Fiber Science, Inc.
245 East 157 Street
Gardena, CA 90248
Attn: E. Dunahoo

General Dynamics
P.O. Box 748
Ft. Worth, TX 76100
Attn: D. J. Wilkins
Library

General Dynamics/Convair
P.O. Box 1128
San Diego, CA 92112
Attn: J. L. Christian
R. Adsit

General Electric Co.
Evendale, OH 45215
Attn: C. Stotler
R. Ravenhall

General Motors Corporation
Detroit Diesel-Allison Division
Indianapolis, IN 46244
Attn: M. Herman

Georgia Institute of Technology
School of Aerospace Engineering
Atlanta, GA 30332
Attn: L. W. Rehfield

Grumman Aerospace Corporation
Bethpage, Long Island, NY 11714
Attn: S. Dastin
J. B. Whiteside

Hamilton Standard Division
United Aircraft Corporation
Windsor Locks, CT 06096
Attn: W. A. Percival

Hercules, Inc.
Allegheny Ballistics Laboratory
P. O. Box 210
Cumberland, MD 21053
Attn: A. A. Vicario

Hughes Aircraft Company
Culver City, CA 90230
Attn: A. Knoell

Illinois Institute of Technology
10 West 32 Street
Chicago, IL 60616
Attn: L. J. Broutman

IIT Research Institute
10 West 35 Street
Chicago, IL 60616
Attn: I. M. Daniel

Jet Propulsion Laboratory
4800 Oak Grove Drive
Pasadena, CA 91103
Attn: Library

Lawrence Livermore Laboratory
P.O. Box 808, L-421
Livermore, CA 94550
Attn: T. T. Chiao
E. M. Wu

Lehigh University
Institute of Fracture &
Solid Mechanics
Bethlehem, PA 18015
Attn: G. C. Sih

Lockheed-Georgia Co.
Advanced Composites Information Center
Dept. 72-14, Zone 402
Marietta, GA 30060
Attn: T. M. Hsu

Lockheed Missiles and Space Co.
P.O. Box 504
Sunnyvale, CA 94087
Attn: R. W. Fenn

Lockheed-California
Burbank, CA 91503
Attn: J. T. Ryder
K. N. Lauraitis
J. C. Ekvall

McDonnell Douglas Aircraft Corporation
P.O. Box 516
Lambert Field, MS 63166
Attn: J. C. Watson

McDonnell Douglas Aircraft Corporation
3855 Lakewood Blvd.
Long Beach, CA 90810
Attn: L. B. Greszczuk

Material Sciences Corporation
1777 Walton Road
Blue Bell, PA 19422
Attn: B. W. Rosen

Massachusetts Institute of Technology
Cambridge, MA 02139
Attn: F. J. McGarry
J. F. Mandell
J. W. Mar

NASA-Ames Research Center
Moffett Field, CA 94035
Attn: Dr. J. Parker
Library

NASA-Flight Research Center
P.O. Box 273
Edwards, CA 93523
Attn: Library

NASA-George C. Marshall Space Flight Center
Huntsville, AL 35812
Attn: C. E. Cataldo, S&E-ASTN-MX
Library

NASA-Goddard Space Flight Center
Greenbelt, MD 20771
Attn: Library

NASA-Langley Research Center
Hampton, VA 23365
Attn: J. H. Starnes
J. G. Davis, Jr.
M. C. Card
J. R. Davidson

NASA-Lewis Research Center
21000 Brookpark Road, Cleveland, OH 44135

Attn: Contracting Officer, MS 501-11
Tech. Report Control, MS 5-5
Tech. Utilization, MS 3-16
AFSC Liaison, MS 501-3
S&MTD Contract Files, MS 49-6
L. Berke, MS 49-6
N. T. Saunders, MS 49-1
R. F. Lark, MS 49-6
J. A. Ziemianski, MS 49-6
R. H. Johns, MS 49-6
C. C. Chamis, MS 49-6 (8 copies)
R. L. Thompson, MS 49-6
T. T. Serafini, MS 49-1
Library, MS 60-3 (2 copies)

NASA-Lyndon B. Johnson Space Center
Houston, TX 77001
Attn: S. Glorioso, SMD-ES52
Library

NASA Scientific and Tech. Information Facility
P.O. Box 8757
Balt/Wash International Airport, MD 21240
Attn: Acquisitions Branch (15 copies)

National Aeronautics & SpaceAdministration
Office of Advanced Research & Technology
Washington DC 20546
Attn: L. Harris, Code RTM-6
M. Greenfield, Code RTM-6
D. J. Weidman, Code RTM-6

National Aeronautics & Space Administration
Office of Technology Utilization
Washington DC 20546

National Bureau of Standards
Eng. Mech. Section
Washington DC 20234
Attn: R. Mitchell

National Science Foundation
Engineering Division
1800 G. Street, NW
Washington DC 20540
Attn: Library

Northrop Corporation Aircraft Group
3901 West Broadway
Hawthorne, CA 90250
Attn: R. M. Verette
G. C. Grimes

Pratt & Whitney Aircraft
East Hartford, CT 06108
Attn: J. M. Woodward

Raytheon Co., Missile System Division
Mechanical Systems Laboratory
Bedford, MA
Attn: P. R. Digiovanni

Rensselaer Polytechnic Institute
Troy, NY 12181
Attn: R. Loewy

Rockwell International
Los Angeles Division
International Airport
Los Angles, CA 90009
Attn: L. M. Lackman
D. Y. Konishi

Sikorsky Aircraft Division
United Aircraft Corporation
Stratford, CT 06602
Attn: Library

Southern Methodist University
Dallas, TX 75275
Attn: R. M. Jones

Space & Missile Systems Organization
Air Force Unit Post Office
Los Angeles, CA 90045
Attn: Technical Data Center

Structural Composites Industries, Inc.
6344 N. Irwindale Avenue
Azusa, CA 91702
Attn: R. Gordon

Texas A&M
Mechanics & Materials Research Center
College Station, TX 77843
Attn: R. A. Schapery
Y. Weitsman

TRW, Inc.
23555 Euclid Avenue
Cleveland, OH 44117
Attn: I. J. Toth

Union Carbide Corporation
P. O. Box 6116
Cleveland, OH 44101
Attn: J. C. Bowman

United Technologies Research Center
East Hartford, CT 06108
Attn: R. C. Novak
Dr. A. Dennis

University of Dayton Research Institute
Dayton, OH 45409
Attn: R. W. Kim

University of Delaware
Mechanical & Aerospace Engineering
Newark, DE 19711
Attn: B. R. Pipes

University of Illinois
Department of Theoretical & Applied Mechanics
Urbana, IL 61801
Attn: S. S. Wang

University of Oklahoma
School of Aerospace Mechanical & Nuclear Engineering
Norman, OK 73069
Attn: C. W. Bert

University of Wyoming
College of Engineering
University Station Box 3295
Laramie, WY 82071
Attn: D. F. Adams

U. S. Army Materials & Mechanics Research Center
Watertown Arsenal
Watertown, MA 02172
Attn: E. M. Lenoe
D. W. Oplinger

V.P. I. and S. U.
Dept. of Eng. Mech.
Blacksburg, VA 24061
Attn: R. H. Heller
H. J. Brinson
C. T. Herakovich
K. L. Reifsnider

End of Document